4-22-2024

Quantifying Landscape Change Using Different Spectrometers, Spectral Unmixing, and UAS Imagery

Bianca Cilento
bmc5922@rit.edu

Quantifying Landscape Change Using Different Spectrometers, Spectral Unmixing, and UAS Imagery

By: Bianca Cilento

A Thesis Submitted in Partial Fulfillment of the Requirements for the Degree of Master of Science in Environmental Science

Thomas H. Gosnell School of Life Sciences
College of Science
Environmental Science Program

Rochester Institute of Technology
Rochester, NY
April 22nd, 2024

Committee Approval:

_____

Carmody McCalley, PhD Date

Chair of Committee, Thesis Advisor

_____

Michael Palace, PhD Date

Committee Member

_____

Karl Korfmacher, PhD Date

Committee Member

Table of Contents

ACKNOWLEDGEMENTS

This research would not have been possible without the support of many influential people and organizations. To begin, I would like to acknowledge the Swedish Polar Research Secretariat, SITES, which is supported by the Swedish Research Council, and the Sámi people for allowing my research to be carried out on their land. I'd like to express my gratitude for the financial support from NSF Grant: DBI-2022070 for funding my travel and boarding throughout the process. Special thanks are extended to the 2022 and 2023 EMERGE REU students and field team members for their assistance in data collection, especially AiLi Pigott, Jes Szetela, Max Murphy, Parker Stoddard, Josibel Pardo, and Helen Sears. I also extend my thanks to those who helped behind the scenes: for image processing- Franklin Sullivan, Christina Herrick, and Sophia Burke- as well as Joseph Cilento for his assistance in hardware construction and optical consulting, Michael Taylor, Paul Mirel, Petya Campbell, Jesse Barber, Ross Walter, Paige Williams, and Nyssa Rayne for STELLA instrument design, Sherwin-William® for ColorSnap® Tool design, and Ruth Varner for EMERGE program development. My biggest thanks goes out to my committee members (Drs. Carmody McCalley, Michael Palace, and Karl Korfmacher), family (Mom, Dad, Joey, Cooper, Oso, and Matt), and friends for their constant support of my ambitions.

LIST OF TABLES AND FIGURES

ABSTRACT

Climate-driven land cover change and biodiversity loss are problems impacting food security, economic growth, human health, and cultural identity of arctic environments, such as Stordalen Mire, Abisko, Sweden (68.35’ N, 18.82’ E). The sensitive nature of these remote areas necessitates large-scale, less-invasive monitoring of environmental change via remote sensing combined with low-impact, cost-effective field validation of remote sensing products. This project assesses the accuracy and utility of two low-cost spectrometers, the Sherwin-Williams® ColorSnap® and the National Aeronautics and Space Administration (NASA) Science and Technology Education for Land/Life Assessment (STELLA-Q), in conjunction with ArcGIS and GoogleEarth Engine programs and aerial imagery to quantify plant species and land cover class changes from 2022 to 2023. This project presents the results of the landscape classifications and land cover change analyses, as well as the tradeoffs of these two devices. The ColorSnap® is an effective tool for collecting spectral data for individual species, while the STELLA is better suited to collect data for land cover class determination. The classifications created from these tools resulted in 77-84% overall accuracy and 0-40% errors of omission and commission. These classifications showed that intact permafrost palsas, are the dominant land cover type at Stordalen Mire, consistently covering just over a third (34-37%) of the landscape in both 2022 and 2023. The introduction of low-cost field portable spectrophotometer tools may allow for increased accuracy and comprehensive analysis of vegetation, which will enable better monitoring of how ecosystems are changing over time.

INTRODUCTION

Biodiversity plays an important, but often overlooked, role in many aspects of daily life, including food security, economic growth/stability, human health, and cultural identity (Badulescu et al., 2019, Laporta et al., 2013). Loss at any level– animals, insects, plants, or microbes– means less resilience and more vulnerability to diseases and pests which could lead to limited food supply, economic collapse, degradation of human health, and reduced cultural identity around the world (Helander-Renvall, 2014). One of the major drivers of biodiversity loss is climate change. This loss may manifest in many ways, including permafrost thaw, which results in arctic ecosystems facing unique, severe challenges. Monitoring the progression of thaw in arctic ecosystems over time will allow researchers to identify patterns and potentially target land management efforts to better protect natural resources and landscapes**.**

Peatlands in subarctic regions underlain by permafrost are experiencing rapid changes in vegetation composition and biodiversity due to permafrost thaw. As permafrost thaw progresses, dry palsa habitats collapse and become wetter, forming Sphagnum-dominated bogs. As thaw continues, the area may become hydrologically connected to surface and groundwater, forming sedge-dominated fens (Malmer et al., 2005, Varner et al., 2022). Plant biodiversity is lost at every stage of the palsa-bog-fen thaw gradient (Figure 1) as fewer plant species are suited for more inundated conditions and in the case of bogs, the low pH associated with high Sphagnum cover. While active layer depth, water table depth, and pH are defining environmental characteristics of each land cover type, species composition is

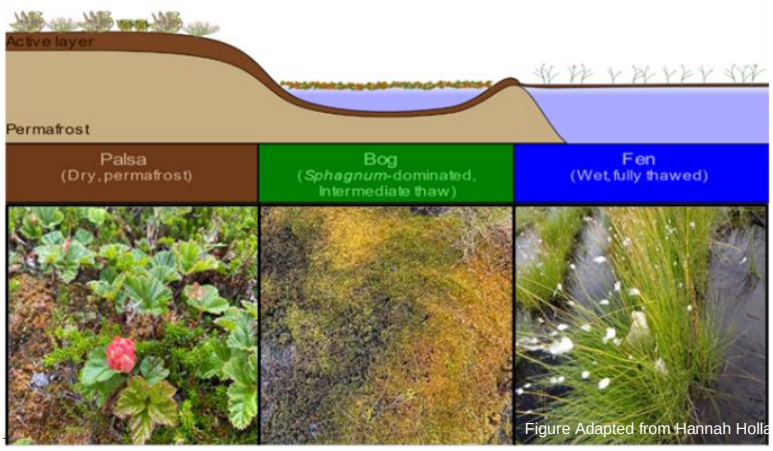

Figure 1 – Thaw Progression: Examples of species found and water content at each stage of thaw found in Arctic

often used when identifying land cover classes in this region, with key species being used to classify land covers along the thaw gradient (Malmer et al., 2005, Malhotra and Roulet 2015). Some species are only found in one of the land cover types due to environmental characteristics that limit their distribution. For example, several sedge species, including *Eriophorum angustifolium* are almost exclusively found in fens whereas high *Sphagnum* moss cover is a key characteristic of bogs (Szetela, 2023, Malmer et al., 2005). Many plants, including *Vaccinium uliginosum* (arctic blueberry), *Empetrum hermaphroditum* (mountain crowberry) and lichens cannot survive wetter conditions and are lost when permafrost thaws (Bienau et al., 2016). It is known that land cover in Stordalen Mire is shifting to become wetter (Varner et al., 2022), so it is important to continue to monitor the rate of change to assess any potential loss of key species not suited to these new conditions.

Monitoring changes in biodiversity over time is critical to ecosystem health assessment as well as scaling changes in ecosystem functions associated with key species. Many subarctic peatlands threatened by climate change in Scandinavia fall on land native to the Sámi people and include plant species that have cultural significance; for example, *Rubus chamaemorus* or cloudberry (Sztela, 2023). Lichen, which disappears completely when permafrost thaw leads to the formation of fens, is an important food source for the reindeer herds managed by the Sámi people (Sandström et al., 2016). Increased cover of tall graminoid species in fully thawed fens is also associated with high rates of methane production and a net positive feedback to warming (Bäckstrand et al., 2010, McCalley et al., 2014, Malholtra et al., 2015, Varner et al., 2022). By monitoring changes in species abundance and distribution over time, areas of high risk can be determined, and management efforts can be put in place such as reducing human-caused disruptions that accelerate thaw. However, traditional monitoring approaches can be costly and time-consuming, and often are stymied by system complexity.

Standard methods of collecting species-presence and change data for monitoring biodiversity include field surveying, which is when researchers use transects to divide and record the composition of every species within a plot. This process is typically

repeated annually, and even multiple times during the growing season to understand how the landscape is changing over time, and it terms of phenology and to create legacy datasets by surveying frequently. Frequent surveying, while extremely important, has the potential to be a very subjective and inconsistent process, based on species knowledge and spatial judgment (Bantilan-Smith et al., 2009). Accessing sites and establishing transects in sensitive ecosystems such as subarctic and arctic habitats may also disrupt permafrost. Measures are taken to address these limitations such as surveying in groups of two or more and relying on identification guides. Another constraint to the field surveying process is its time-consuming and expensive nature, especially over a large study, which can be addressed by using remote sensing.

The introduction of remote sensing for vegetation and biodiversity monitoring allows for practical, cost-effective, large-scale data collection. Habitat assessment through aerial imagery offers an alternate approach for monitoring changes in land cover, species composition and biodiversity loss, while minimizing damage to the environment. Remote sensing and aerial imagery can be used to monitor the different characteristics of a landscape including vegetation index, water content, and land cover change. Arctic studies have been able use remote sensing methods to show warming trends and permafrost collapse across the site (Palace et al., 2018). These classification maps may be made using unsupervised or supervised methods, meaning without or with the inclusion of training sites, which can be collected in-person at the site or selected in the aerial image.

Accuracy of aerial assessment can be improved through the use of hand-held, field-portable spectrometers such as the Spectra Vista Corp. (SVC) or Analytical Spectral Device (ASD), which are considered industry standard for spectral signature collection and endmember creation, and two potential alternatives: the Sherwin-Williams® ColorSnap® Tool and the NASA STELLA-Q. SVC and ASD spectrometers come in a range of sizes and measure reflectance continuously across the electromagnetic spectrum, which results in a large dataset that can be unwieldly and time consuming to analyze. While having reflectance measurements over a larger range of wavelengths can be an advantage to using a spectroradiometer, it can also provide

for an overwhelming sample size and can make the data difficult to decipher. Industry standard spectrometers may also be expensive, cumbersome to handle in the field, and collect point-based spectra, making them inaccessible to many researchers. Both the Sherwin-Williams® ColorSnap® Tool (Figure 2) and the NASA STELLA-Q (Figure 3) are simplified, but powerful alternatives that have the potential to provide high quality data in a field portable, cost-effective package.

The Sherwin-Williams® ColorSnap® Tool was designed to measure the reflectance of paint colors and correctly identify the name of the paint used and provide the ability to match existing paint. The device connects via Bluetooth to a mobile app for display and comes with a pure-white calibration cap, built-in light source, and a pinhole diameter of 4mm. Measurements are taken by completely covering the aperture and not letting in other light to achieve a constant illumination condition. Three signature values are displayed as digital numbers in the blue, green, and red region of the electromagnetic spectrum. The small pinhole size and collection methods of this tool makes the ColorSnap® ideal for the collection of spectral signatures of individual plant species.

Figure 2 - ColorSnap®: Tool and Sherwin-Williams® ColorSnap® App

NASA's STELLA, (Science and Technology Education for Land/Life Assessment), has multiple versions to best fit the spectral needs of the researcher, all of which were designed by Paul Mirel. This project used the STELLA-Q, which collects 11 unique bands ranging from 450-860nm, each with a 5nm range. (See *Appendix A* for specific wavelengths). This device has a larger pinhole, resulting in a greater field of view, making it more suitable for land cover classification based on plant community composition.

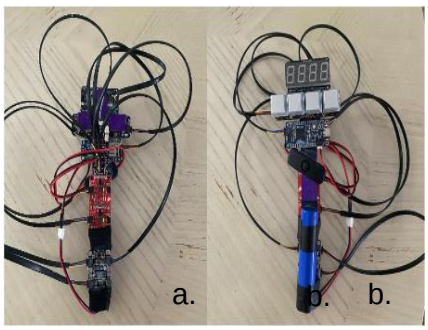

Figure 3a and 3b – NASA STELLA-Q: Images of the front and back of the STELLA. In this case, the front (left) is identified as the side with the sensors and the back (right) has the screen and buttons.

This project used the ColorSnap® and STELLA devices to create a collection of known reflectance values at different wavelengths for a specific endmember (pure samples) under constant illumination conditions, so as to not be impacted by atmospheric noise such as cloud cover or haze, called a spectral library. Such endmembers typically are collected with a spectroradiometer. Given the differences in the diameter of the sensors, the ColorSnap® was used to collect spectral signatures for plant species, while the STELLA was used to collect spectral data with different land cover classes as the endmembers. With these devices, we proposed to simplify classification approaches that continuously cover the Visible, RedEdge, Near Infrared (NIR), and Shortwave Infrared (SWIR) spectral ranges (Costa et al., 2022), to only focus on small ranges of each section of the EMR. This approach has the advantage of using a smaller spectral range which yields a reduced sample size and provides a tractable dataset while still covering the major regions of the EMR.

This research compared a variety of combinations of aerial imagery, field collection tools, and classification methods to monitor and quantify landscape changes in sensitive environments as well as efficiently and accurately predict potential areas of loss in the future. The Sherwin-Williams® ColorSnap® tool and NASA STELLA Q tools tested in this study can improve biodiversity and climate change research by enabling researchers to monitor plant species changes without significantly disrupting arctic ecosystems.

METHODS

1.1 Study site

This study was conducted at Stordalen Mire in Abisko, Sweden (68.35’ N, 18.82’ E), a sub-arctic peatland in the discontinuous permafrost zone (Figure 4) that is experiencing biodiversity losses and changes in carbon cycling due to permafrost thaw (Malmer et al., 2005, Varner et al., 2022). Stordalen Mire has a long history of environmental research ranging from ecology to remote sensing with a focus on understanding the effects of climate change on ecosystem structure and function (Jonasson et al., 2012). Land cover has been changing in Stordalen Mire drastically since first recorded in 1970, with palsa populations decreasing by 11% between 1970-2014 (Varner et al., 2021). Landscape changes in Stordalen Mire can be especially detrimental as permafrost thaw leads to a shift in vegetation and hydrology to wetter land covers (Johansson et al., 2006). Continued monitoring of these changes can show if the rate at which land cover is changing is increasing as climate change progresses.

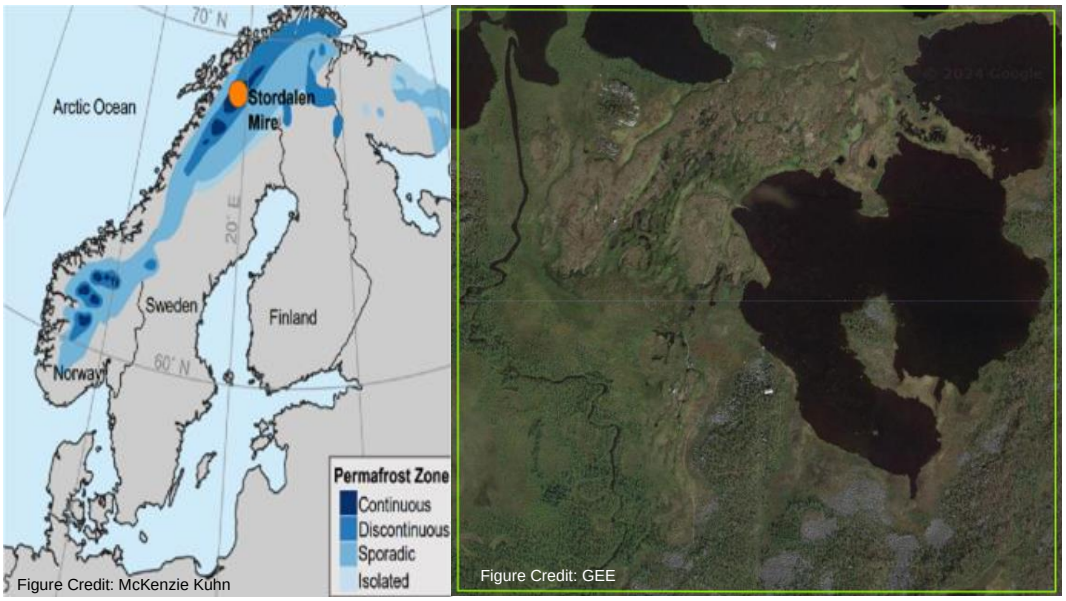

Figure 4 – Map of Study Site: Location of Stordalen Mire in Abisko, Sweden and the distribution of Permafrost Zones.

1.2 Sherwin-Williams® ColorSnap® Tool and NASA STELLA-Q

Endmember spectral signatures collected by the Sherwin-Williams® ColorSnap® tool and NASA STELLA were analyzed in a few different ways to maximize data usage. One approach was to create a species composition map of Stordalen Mire by reclassifying pixels of an unmanned aerial system (UAS) imagery. Literature shows that these analyses can be used for land cover and vegetation classification across years if collection factors are consistent (Berberoglu, 1999). To quantitatively analyze the accuracy of the species composition map, species composition was determined in the field at ground truth sites. A Kappa-hat analysis was used to show not only the overall accuracy of the model, but also which species had the highest omission or commission error, i.e., which species are most frequently missed or overestimated (Choi et al., 2021). Kappa Statistic is generally a polarizing metric as in some cases it may be misleading or flawed (Pontius et al., 2011), but this analysis does not have a dominant cover classification to improperly skew the results, so it was an appropriate metric of accuracy for this project.

1.3 Aerial Image Collection, Processing, and Calibration

Aerial imagery of Stordalen Mire was collected with a DJI Phantom 4 Drone a 5-band camera collecting at 450nm, 560nm, and 650nm in the visible range, 730nm in the RedEdge, and 840nm in the Near-infrared regions of the EMR. Drone flights occurred in mid-July of 2022 and 2023, during peak growing season at Stordalen Mire, and drones were flown between 70-80 meters to achieve 7-cm spatial resolution. While flying, the drone took 2-3 images per second and the images were later stitched together based on location information collected using a Real-Time Kinematics (RTK) system.

A two-toned, Group 8 Technology© calibration tarp was flown over and included in the final images to translate the endmember values collected by the drone in the air to the handheld spectrometer on the ground (Figure 5). A half light gray and half dark gray tarp was used. The tarp was scanned 30 times on each side of the tarp with the ColorSnap®, moving it around to reduce any bias or error. Additionally, the STELLA was used to collect another 30 spectral measurements on each side, following the same endmember collection criteria. The signatures collected were then averaged to determine the endmember value of the light and dark gray sections of the tarp. The RGB and reflectance values determined by the drone were different from those collected by the drone in the field because there is more atmospheric noise (Griffy, 1989). To account for that noise, the RGB values were translated to match the ColorSnap® and STELLA values using the calibration tarp as reference for the correction equation.

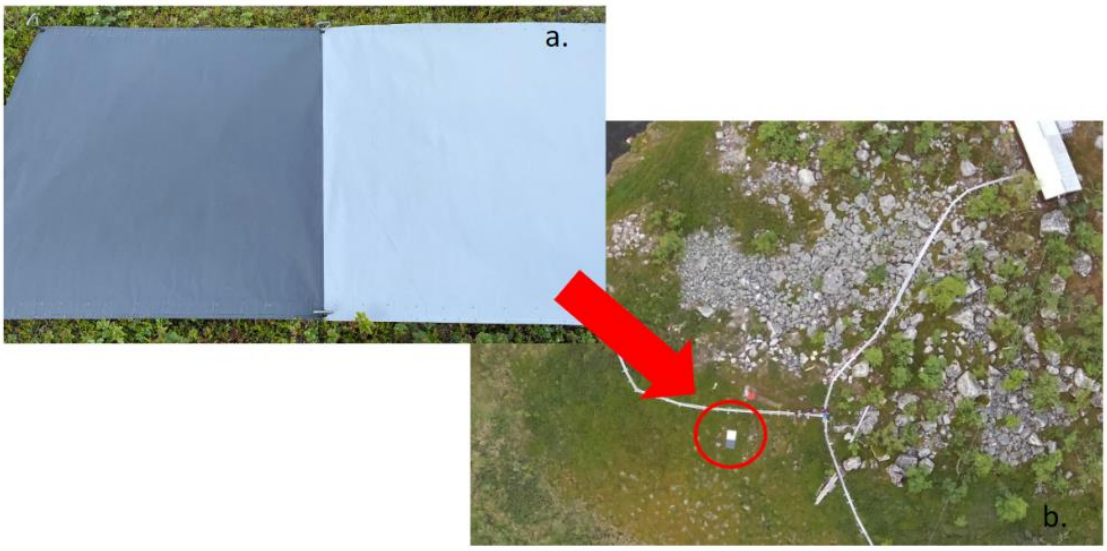

Figure 5– Group 8 Calibration Tarp seen in on the ground (a) and from the drone (b): Ground image (a) and Aerial image of Group 8 Calibration tarp to show the visual differences that occur at different altitudes, thus need to calibrate.

1.4 Field Surveying

While collecting spectral measurements, field surveying was done to identify species composition and the land cover type (palsa, bog, fen, open water) based documented characteristics of each of these habitat types (Figure 1, Malmer et al 2005). Palsas are elevated areas of intact permafrost with a variety of plant species present

(*Appendix B),* bogs are sphagnum-dominated and ombrotrophic, and fens have high sedge cover, no permafrost and a water table at or above the peat surface. Open water was also included as a land cover type, identified as areas with little-to-no canopy cover. Field surveying was done across 70 sites in 2023 and each was categorized as either palsa, bog, fen, or open water (Figure 6). These sites were picked as part of a 2015 Mire-wide study where species composition, hydrology, and other important ecological features were studied. The same sites were used for ground truthing in 2022, using an aerial identification of land cover type which was possible due to the high spatial resolution of the drone imagery and the distinct visual characteristics of the land cover types (Palace et al. 2018).

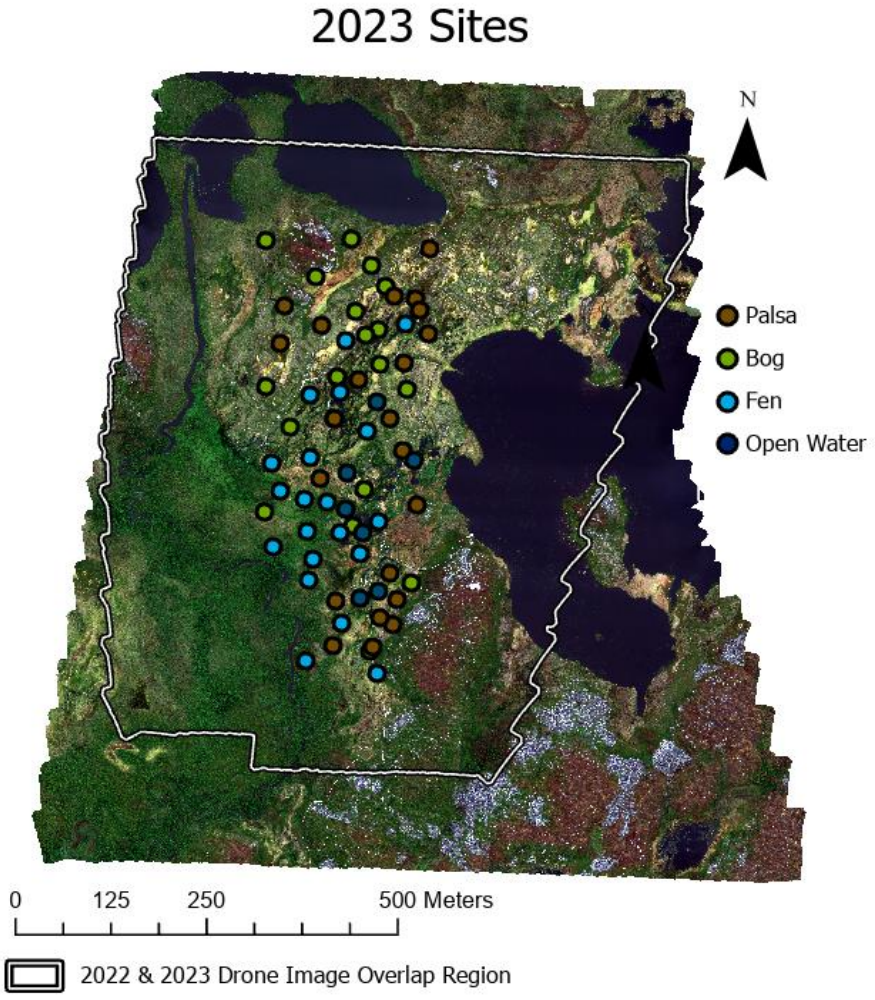

Figure 6– Field Surveying and Ground Truth Sites: Location and classification of 2023 plots. There are 24 palsas, 20 bogs, 19 fens, and 7 open water sites. White outline represents the overlap between 2022 and 2023 drone images.

1.5 ColorSnap® -- Ground Truth and Endmember Collection

Ground truth and endmember measurements for the ColorSnap® Tool were collected at separate plots due to the destructive nature of species-level endmember collection. For ground truthing, nine sites were set up per land cover type (open water was omitted due to the lack of plant species), with three 1.0x1.0m plots at each site. This resulted in a total of 27 total ground truth sites used for species composition ground truthing in 2022. Endmember collection using the ColorSnap® is an invasive, destructive process, so it required separate sites so as to not disrupt other phenology or composition monitoring happening at the ground truth sites. Endmember collection sites were set up in a 5.0x1.0m plot across the boardwalk from each ground truth site (Figure 7). Thirty-one different endmembers (*Appendix B)* were collected including fifteen plant species across different stages of their phenological cycles, rocks, boardwalk, and soil/bare earth, with thirty measurements taken per endmember.

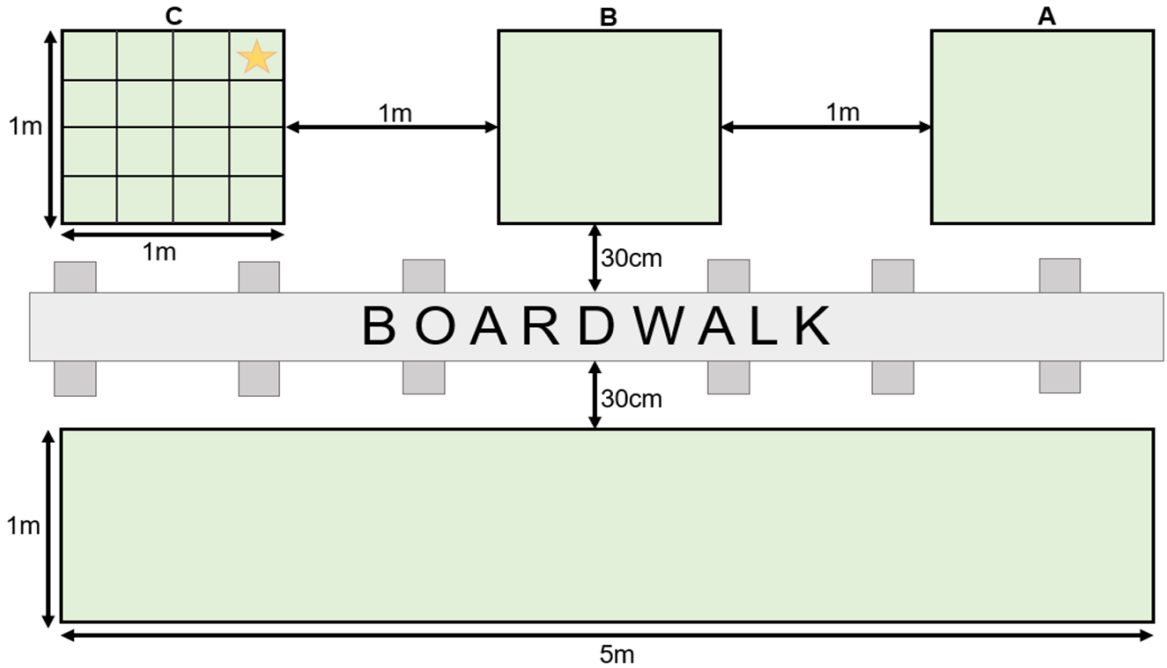

Figure 7 – **ColorSnap® Plot Set up -** Field set-up for ColorSnap® ground truth and endmember collection. Three sets of 1x1m plots aligned along a 5m transect were set up across a 5x1m plot.

1.6 STELLA -- Ground Truth and Endmember Collection

Ground truth and endmember collection using the STELLA was done in the same 70, 1mx1m plots: 24 palsa, 20 bogs, 19 fens, and 7 open water sites (see Figure 8a), where the corners and centers were both recorded several times using a handheld GPS. To collect spectral readings at each site, the STELLA device was held 1.0m above the center of each ground truth plot and the total area collected by each measurement was 0.416m^2 (see Figure 8b). Forty-five measurements were taken at each plot and then averaged to create a single value for that plot.

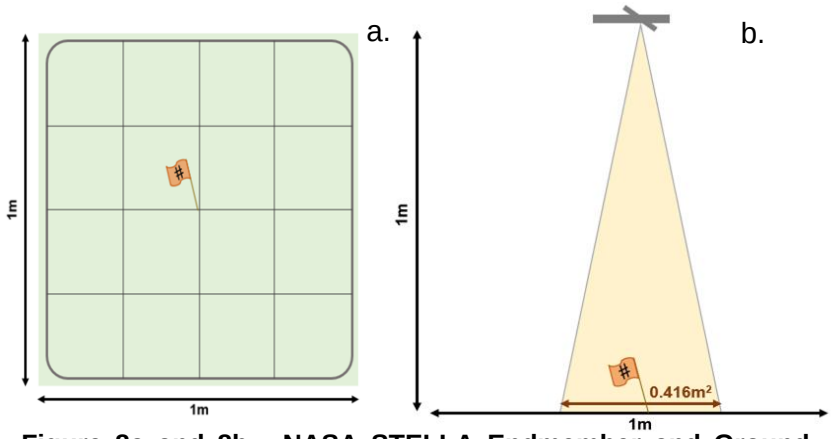

Figure 8a and 8b - NASA STELLA Endmember and Ground Truth Collection: The device was held 1m above the center of each 1x1m study site plot to collect a 0.416m^2 area centered over the plot where vegetation surveys were conducted.

1.7 Statistical Analysis

Two methods were used to determine the separability between and within each endmember, which allowed for predictions of which classes would be the most difficult to distinguish and might need additional samples collected, as well as identification of closely related species that were spectrally similar and needed to be grouped at the genus level for analysis. Additionally, these results indicated which wavelengths were key for identifying endmembers. For preliminary results, cluster analyses were done using JMP Pro (Version 16.2.0, SAS Institute, 2020-2021). A discriminant function analysis (DFA) was performed to visualize this information. Zonal Statistics were run in ArcGIS Pro (Version 3.2.0, ESRI, 2023) to calculate the average, range, and standard deviation of the reflectance for the sites within each cover type category.

1.8 Reclassification

1.8.1 Google Earth Engine

Google Earth Engine (GEE) (Gorelick et al., 2017) was used to classify the drone images in 2022 and 2023 based on the endmembers collected by the ColorSnap® and STELLA devices, respectively. While the classification levels were different, the methods stayed consistent. The drone images were loaded into GEE and code was developed using the image.unmix feature to classify each image based on the assigned endmember values found by each device. Spectral unmixing is a process in remote sensing used to determine the composition of a pixel based on endmember values (Bioucas-Dias et al., 2013, Roberts, 1991). Unmixing essentially deconstructs each pixel to determine the composition of each species or land cover type and reassigns the pixel as the most prominent (Shi, 2015). The spectral unmixing code used can be found in *Appendix C*. The mosaicked image collected by the drone was uploaded to GEE and the endmember species and values were added as variables. In order to compare both classification methods, a second reclassification was done to the 2022 species-level map that assigned a suitable land-cover type to each species (*Appendix B)*, creating a land cover map.

1.8.2 ArcGIS

ArcGIS Pro (Version 3.2.0, ESRI, 2023) has built-in classifiers which can be used without requiring ground-level calibration, as reference plots are recorded with the same sensor, under the same atmospheric and collection conditions. For this analysis, a Random Trees classifier was used. Only land cover level classification was done in ArcGIS as the aerial image resolution was not high enough for species-level classification using this method. The 2023 drone image and GPS points marking the corners and center of the ground truth plots were added into ArcGIS for this analysis. Seventy Feature Collections were made by connecting the corners of each plot for each land cover type and using the 1x1 meter areas as the training sites for a Supervised Classification. For ground-truth verification, the center point of each plot was used.

1.9 Accuracy Analysis

Before using classification maps for further analyses, it was imperative to determine their accuracy. In addition to quantifying overall accuracy (proportion of correct classification of ground truth sites), we used several methods for calculating the success of map classification that looked at different factors associated with accuracy. We used the Kappa statistic, or k-hat, as the major metric for accuracy, as it quantifies how an analysis compares to a random classification (see Eq. 1). While there is some variation across studies, values above 0.6 are generally considered successful or 'good' classifications (McHugh, 2012).

$$K_{hat} = \frac{N\sum_{i=1}^{r} x_{ii} - \sum_{i=1}^{r}(x_{i+} * x_{+i})}{N^2 - \sum_{i=1}^{r}(x_{i+} * x_{+i})} \qquad \textit{Equation 1}$$

Omission and commission errors for each class were also calculated to find which species or land cover types were distinguishable from each other and which were easily confused in the model. Commission Error specifically targets when classes are overestimated by dividing the total number of correct classifications of an endmember by the total number of sites classified as that cover type (see Eq. 2). Error of omission uses reference points and correctly identified points to show error from incorrectly excluded data (see Eq. 3). A combination of these accuracy measures were used for a well-rounded and unbiased analysis.

$$\textit{Error of Commission (User Accuracy)} = 1 - \frac{Correctly\ Identified\ Points\ per\ Category}{Classified\ Points\ per\ Category} \qquad \textit{Equation. 2}$$

$$\textit{Error of Omission (Producer Accuracy)} = 1 - \frac{Correctly\ Identified\ Ponits\ per\ Category}{Reference\ Points\ per\ Category} \qquad \textit{Equation. 3}$$

1.10 Cover Type Changes

1.10.1 Land Cover

Quantifying land cover changes between 2022 and 2023 was done in ArcGIS using the classification maps made using the STELLA-collected data. Maps with area classified into four land cover classes (palsa, bog, fen, open water) from 2022 and 2023 were clipped to the same size based on their overlapping areas. The Combine tool was then used to create 16 new classes showing all possible combinations of land cover change between the two years. These new classes were then recategorized into 3 categories: land cover changes that follow thaw progression, land cover changes that go against thaw progression and no change. The total number of pixels in each new category were then multiplied by the pixel area to quantify the total amount of land cover change, loss, and gain, between 2022-2023.

1.10.2 NDVI

Normalized Difference Vegetation Index (NDVI) is a metric for quantifying the presence of photosynthetically active plant material, which can be used to quantify changes in vegetation over time (Huang et al., 2011). This change detection software is built into ArcGIS Pro and utilizes the red and NIR bands of the drone image (see Eq. 4). NDVI is measured on -1 to 1 scale, typically with anything above 0 being capable of photosynthesis and lesser values are typically too moisture stressed for photosynthesis. Photosynthetic material such as plants, can also be visualized using the red and NIR bands as red and everything else is displayed as a teal to black gradient. The 2022 and 2023 images were input as the ‘From Raster’ and ‘To Raster,’ respectively to calculate changes in NDVI. Areas with at least 50% change were selected to show significant changes.

$$NDVI = \frac{(NIR - Red)}{(NIR + Red)} \qquad \textit{Eq. 4}$$

1.10.3 Species Change

In addition to quantifying vegetation change based on changes in land cover and NDVI, quantifying the loss of key species can be a powerful way to monitor habitat changes. Using the ColorSnap® tool, the presence and distribution of specific species can be identified and monitored over time. For this analysis, we focused on lichen cover at Stordalen Mire due to its sensitivity to warming (Bao et al., 2022), its role as a key food source for reindeer (Inga, 2007) and its unique spectral characteristics. Using GEE and the ColorSnap®-collected species endmembers, the presence of lichen was displayed on a white-black gradient for visualization purposes (*Appendix D).* Additionally, an alternative to Boolean maps showing the range of lichen across Stordalen Mire was created by selecting pixels with at least 10% lichen composition and the total area of lichen was calculated for 2022 and 2023 and used to quantify changes in lichen cover between years.

RESULTS AND DISCUSSION

2.1 Aerial Imagery

The final, mosaicked, 5-band images of Stordalen Mire collected in 2022 and 2023 have 7-cm pixel resolution (Figures 9a and 9b). Images were collected in late June in their respective years to accurately capture land cover changes in peak growing season.

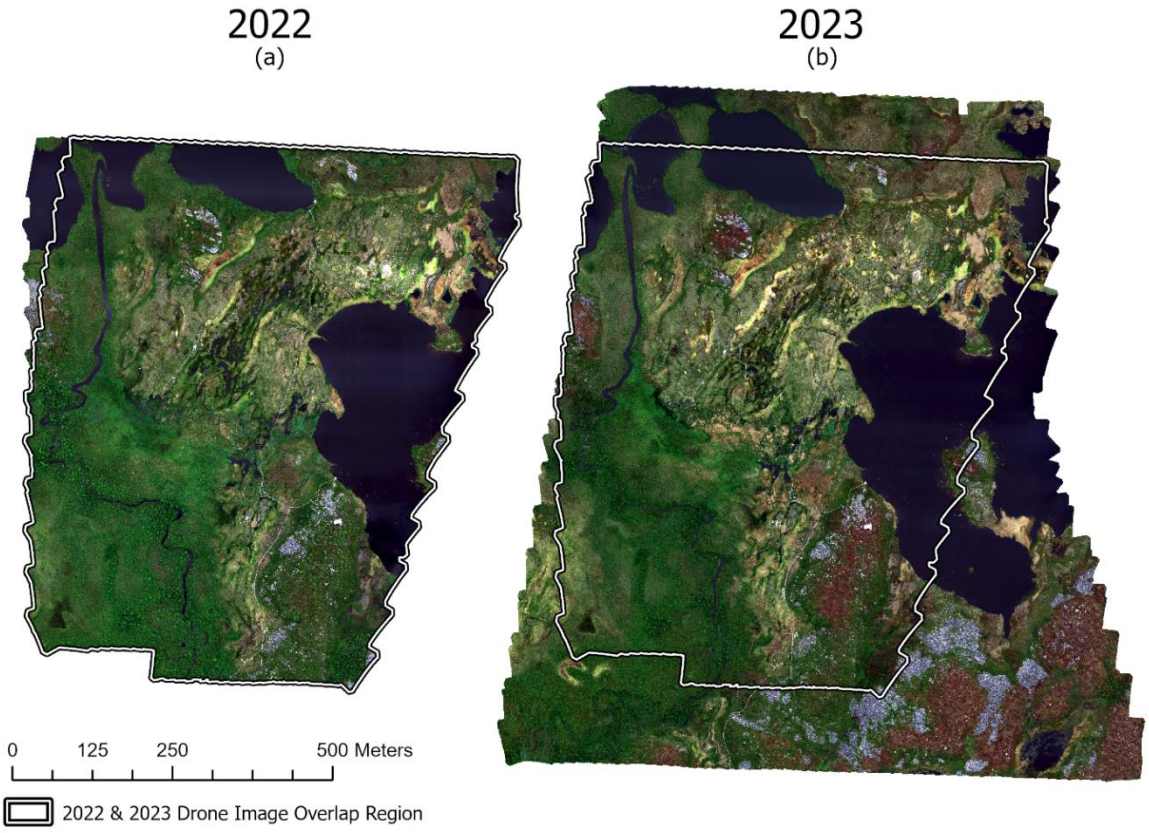

Figure 9a and 9b: Aerial Imagery of Stordalen Mire - Mosaicked images of Stordalen Mire in 2022 (9a) and 2023 (9b).

2.2 Endmember Separation

The separability within and between species (ColorSnap) and land cover classes (STELLA) analyzed in JMP provided preliminary results showing which endmembers would be the most difficult for the model to distinguish from one another.

ColorSnap

There was significant overlap between a majority of the species measured with the ColorSnap® (Figure 10). The results of the DFA are 24 misclassified species out of the 132 training samples, resulting in an 18.2% misclassification rate. The species with the most unique signature was *Rubus chamaemorus* leaves, which is expected, given its red color throughout the majority of growing season. The Red band was the most useful in distinguishing between species, and the Green band was the least useful. This is likely due to the high greenness across most of the species.

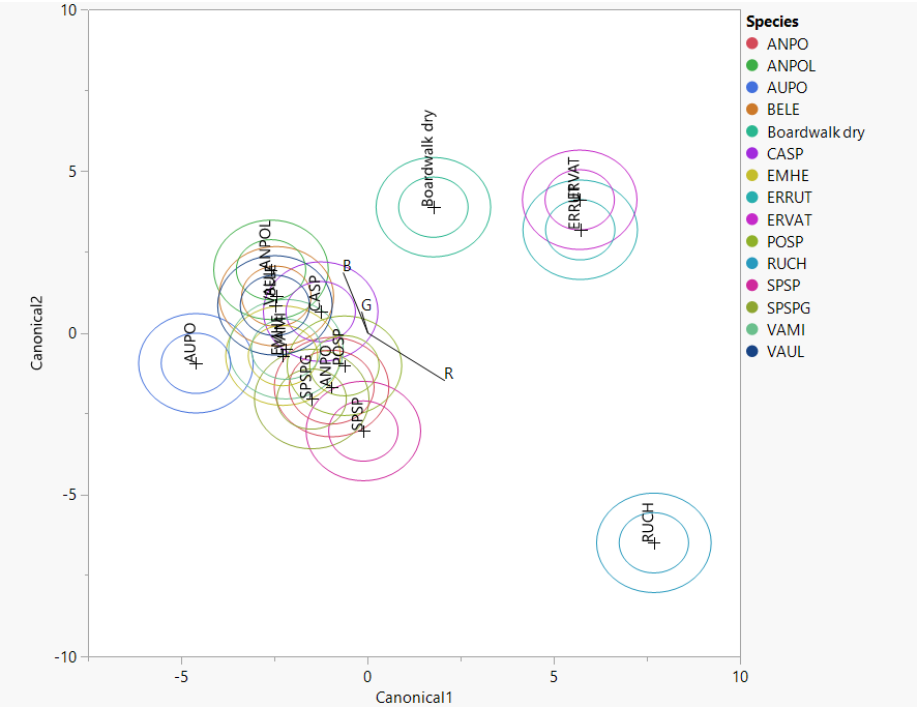

Figure 10: Separation between endmembers based on Red, Green, and Blue regions of the EMR collected with the ColorSnap® - Several plant species have similar spectral signatures and heavily overlap each other, but key species can be easily identified such as *Rubus chamaemorus.*

STELLA

The separability between the four land cover types was visualized in two different ways: a DFA and Reflectance vs. Wavelength plot (Figure 11). Model verification was done with 47 of the sites and yielding 87.2% overall accuracy. Both figures visualize the same results, there is not a lot of overlap between the different land cover spectra, but palsa and fens are the most similar; therefore, the most difficult to separate. In the DFA, there are two rings displayed for each cover type, with the innermost representing a 50% confidence interval (CI) and the outer a 95% CI for a classification. The overlap between palsas and fens is minimal when only using the 50% CI, but it is more apparent using the 95% CI.

The overlap may occur for many reasons, but two of the most are that there is spectral spectral similarity between dominant plant species found at palsas and fens or that there is another, transitionary phase of the thaw progression that is not included in our study. *Eriophorum vaginatum* is commonly found in palsa and *Eriophorum angustifolium* is typically found in wetter areas like fens, but they are visually and spectrally very similar, which can lead to spectral similarities between those land cover types. Another reason for this overlap could be sites collected at ‘in-between’ land covers that are in the process of thawing. Additionally, there is a land cover type not used in this analysis, described as ‘tall shrub,’ consisting mostly of willow and birch shrubs, located in the South West portion of Stordalen Mire (Palace et al 2018). This cover was excluded in this analysis as it is not part of the permafrost thaw progression and is mostly found on the outskirts of the research site. It is possible that the inclusion of tall shrubs may improve the accuracy and reduce the overlap between palsa and bog land covers.

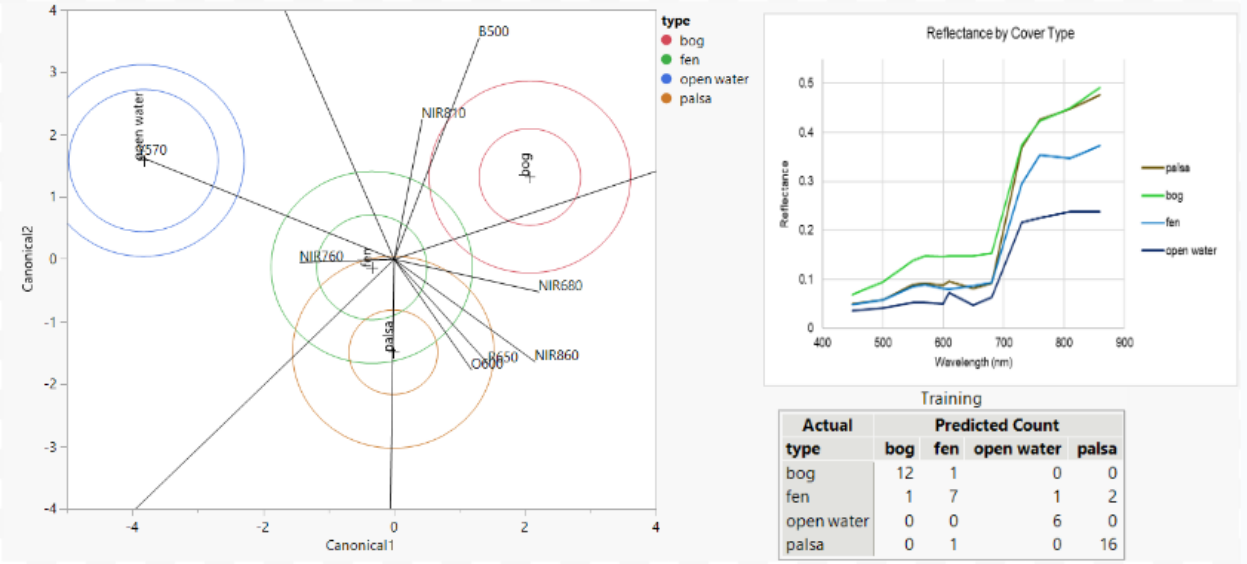

Figure 11: Separation between land cover signatures based on each wavelength region collected by the STELLA - The easiest class to distinguish is Open Water as it has the most unique signature, and the most difficult are Palsa/Fen as they have the most overlap.

2.3 Reclassification

Accuracy of the classification maps created using spectral unmixing in GoogleEarth Engine depended mostly on the tool used for endmember collection. Land cover classifications using species-level data collected with the ColorSnap® had, on average, lower accuracy and higher error than those created with the land cover data from the STELLA.

2.3.1 GEE: ColorSnap®

Determining the accuracy of the species-level classification map (Figure 12) is difficult, as the spatial resolution is too coarse to show the full extent of species presence, so a second-level classification was done based on which land cover type the most prominent species can be found in. This was done by reclassifying the species into their associated land covers. See Appendix B for this list. The land cover map created with the ColorSnap® (Figure 13) had the highest misclassification rate of 46%, which is expected given the spectral capabilities of the tool. The k-hat of this analysis is 0.473, indicating poor agreement between the model and actual records, and there is not much improvement compared to a random classifier (Table 1). Due to the low

accuracy of the 2022 classification map, this analysis was not repeated on the 2023 drone image.

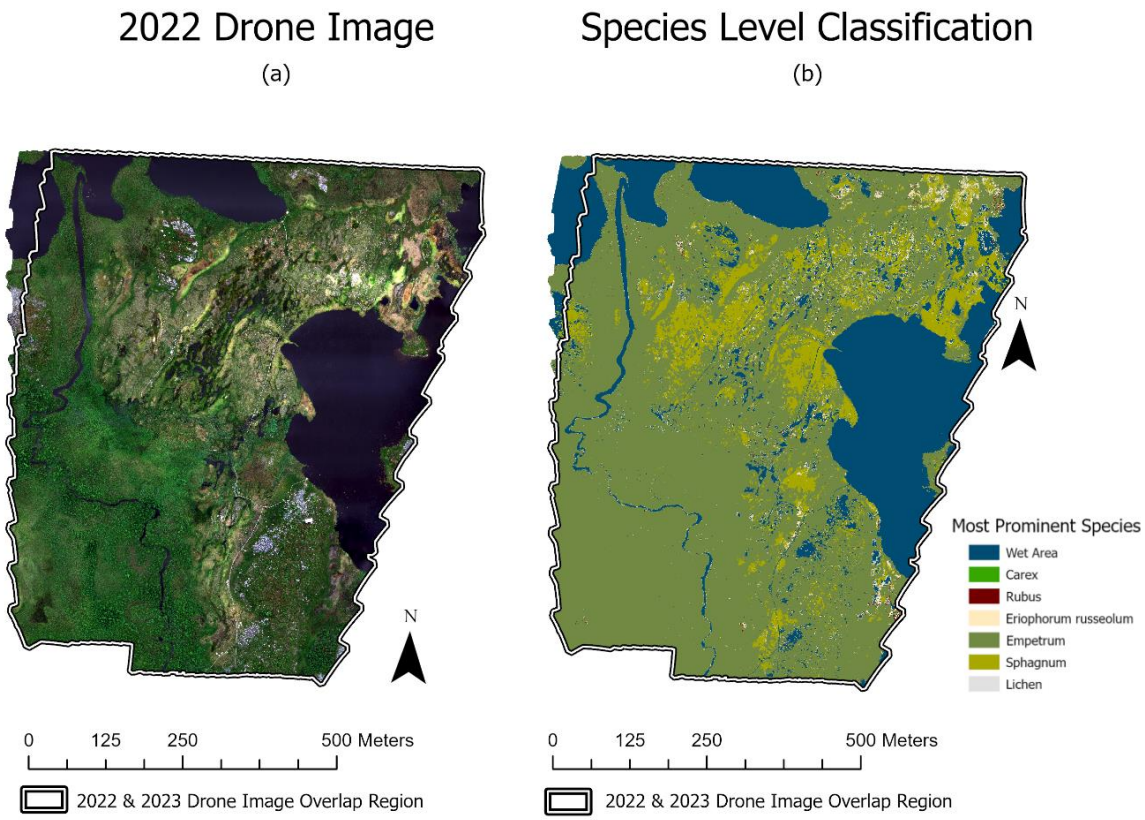

Figure 12a and 12b: Species Level Classification (12b) of 2022 Drone Imagery (12a) - Species-level reclassification of June 2022 image of Stordalen Mire. While there were 31 endmembers included in this analysis, only 7 were identified as the most prominent in a pixel.

Species to Land Cover (ColorSnap)

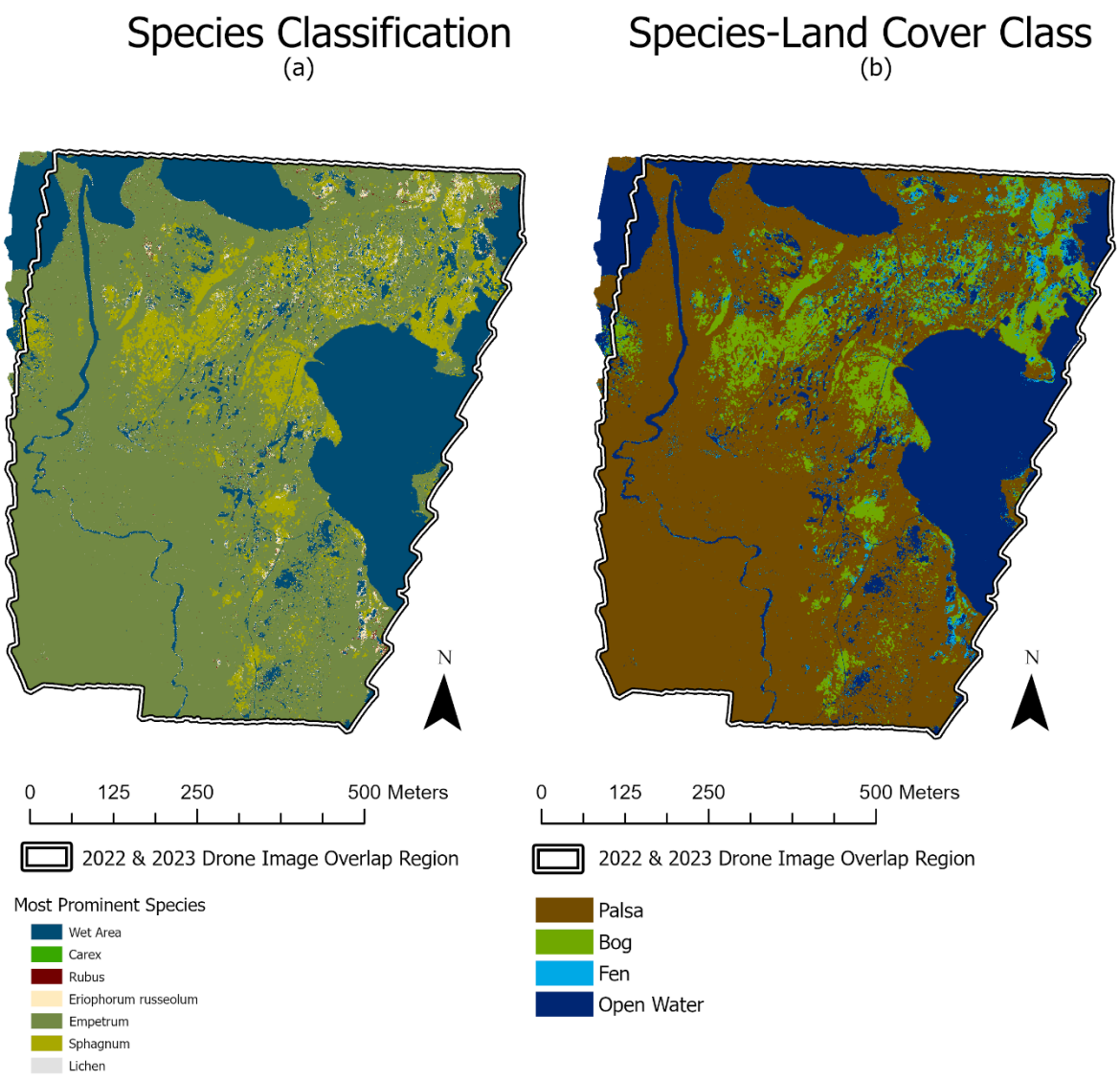

Figure 13a and 13b: Species to Land Cover Classification using the ColorSnap® - Based on the species-level spectral unmixing of the 2022 drone imagery, another classification map was assigning species into the land cover types they can be found. Due to the similarity and misclassification between palsa and fen species (*Eriophorum* sp.), there are a lot of omitted fen sites and overestimated palsa sites.

Table 1: Accuracy of 2022 Species to Land Cover Classification –
Classification accuracies for 2022 land cover map created using GoogleEarth Engine. The overall accuracy of this analysis was 64.3%, with the largest reason for this low classification being the overestimate of palsa sites and underestimate of bog sites.

		Classification				
		Palsa	Bog	Fen	Open Water	Total
Reference	Palsa	23	1	1		25
	Bog	9	9	1	1	20
	Fen	10		11		21
	Open Water	1		1	2	4
	Total	43	10	14	3	70

	Producer Accuracy	Consumer Accuracy
Palsa	92.00%	53.49%
Bog	45.00%	90.00%
Fen	52.38%	78.57%
Open Water	50.00%	66.67%
	K-Hat	0.473
	Overall Accuracy	0.643

2.3.2 STELLA

Land cover classification using the STELLA collected records were done using both 2022 and 2023 imagery (Figures 14a and 14b), yielding similar accuracy results, with the 2022 having a slightly lower overall accuracy and k-hat value, 71% and 0.8, respectively (Table 2). The results of the 2022 accuracy are just above with an overall accuracy of 78% and a k-hat value 0.84 (Table 3). These values indicate a substantial, near-perfect agreement between training and truth points, and these models are much better compared to a random classifier.

The most noticeable change between the 2022 and 2023 land cover classifications is the amount of the change from palsa to fen sites. There are several potential reasons for this change, with the seemingly most obvious being that the

landscape is shifting to wetter conditions and permafrost is thawing. This drastic change, while possible, is more likely attributed to the conditions of Stordalen Mire when the aerial images were collected. In 2022, the mire was abnormally wet, but 2023 was one of the driest years in the mire's recent history. Since all the spectral data for the land covers were collected in 2023 and given the spectral similarity between palsas and fens seen in Figure 11, it is likely that the model confused the drier fen sites of 2023 with the uncharacteristically wet palsa sites in 2022. While image calibration was done to try to minimize the impact of environmental factors in this analysis, there will be slight natural variations between dates and years. This highlights the importance of repeat monitoring to account for these types of anomalies or variations of environmental conditions and ensure the most accurate classification.

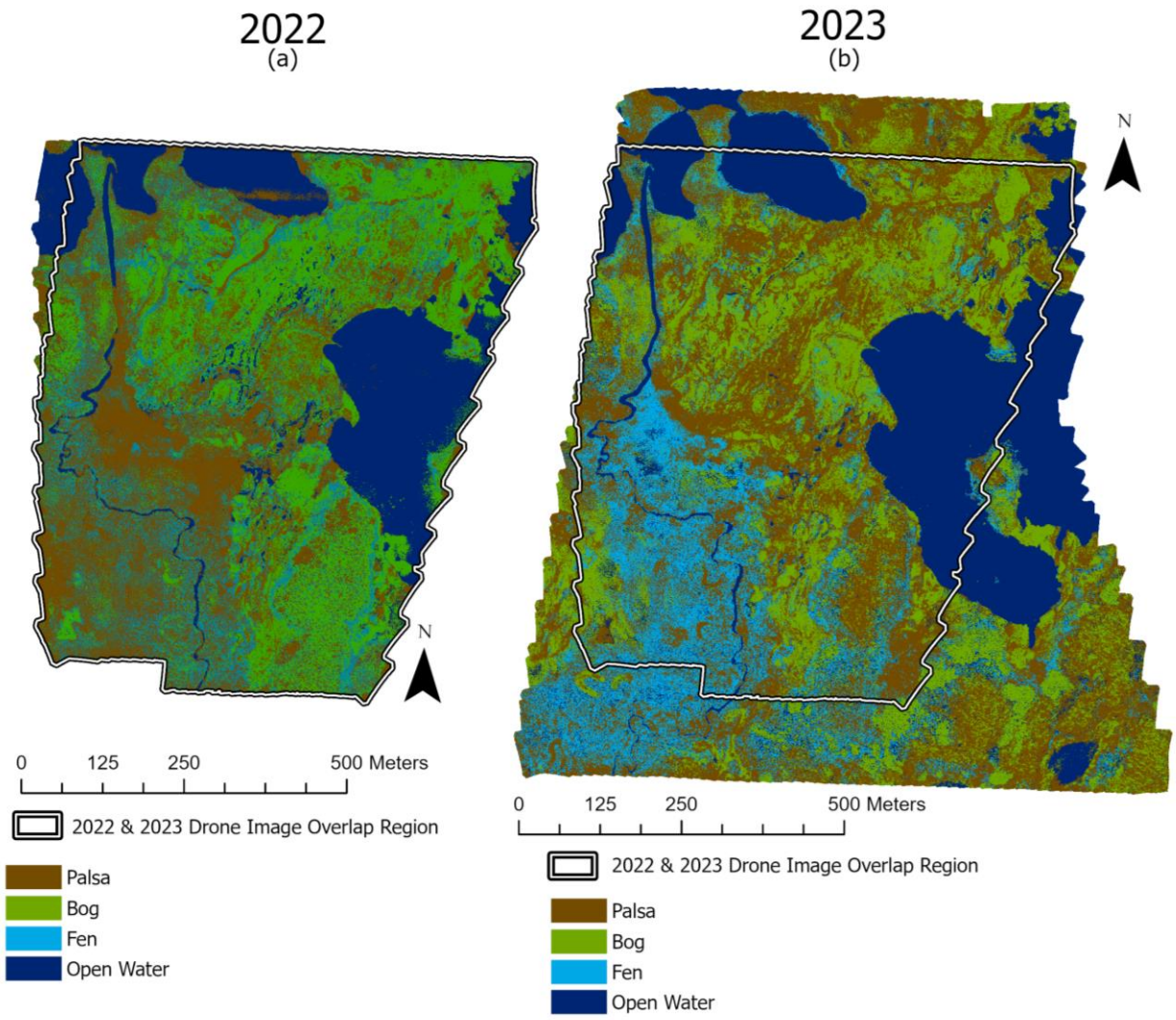

Figure 14a and 14b: Classified 2022 and 2023 of Stordalen Mire made in GEE using STELLA endmember collection - Reclassified drone images created from the average reflectance in the red, green, blue, RedEdge, and NIR regions on the EMR collected using the STELLA.

Table 2: Accuracy of 2022 Reclassification Map made in GEE –

Classification accuracies for 2022 land cover map created using the STELLA and GoogleEarth Engine. The overall accuracy of this analysis was 80%, where Open Water accounts for the 'most' producer and consumer error given its low number of samples.

		Classification				
		Palsa	Bog	Fen	Open Water	Total
Reference	Palsa	21	2	2		25
	Bog	1	16	2	1	20
	Fen	4		16	1	21
	Open Water			1	3	4
	Total	26	18	21	5	70

	Producer Accuracy	Consumer Accuracy
Palsa	84.00%	80.77%
Bog	80.00%	88.89%
Fen	76.19%	76.19%
Open Water	75.00%	60.00%
	K-Hat	0.714
	Overall Accuracy	0.80

Table 3: Accuracy of 2023 Reclassification Map made in GEE –

Classification accuracies for 2023 land cover map created using the STELLA and GoogleEarth Engine. This method has the highest overall accuracy at 84%, with the most misclassifications accounting from the overprediction of palsa sites.

		Classification				
		Palsa	Bog	Fen	Open Water	Total
Reference	Palsa	20	1	3		24
	Bog	3	17			20
	Fen	2	1	15	1	19
	Open Water				7	7
	Total	25	19	18	8	70

	Producer Accuracy	Consumer Accuracy
Palsa	83.33%	80.00%
Bog	85.00%	89.47%
Fen	78.95%	83.33%
Open Water	100.00%	87.50%
	K-Hat	0.781
	Overall Accuracy	0.84

2.3.3 ArcGIS

Land cover classifications of the 2022 and 2023 drone imagery created without the use of endmembers collected with field spectrometers in ArcGIS (Figures 15a and 15b), had similar accuracy to each other, but lower than the maps created with the STELLA data. The 2022 map had an overall classification rate of 77% and a k-hat of 0.676 (Table 4), and the 2023 map's overall accuracy and k-hat of 78% and 0.701, respectively (Table 5). These accuracy values are indicative of a moderate to substantial classification, well above a random classifier.

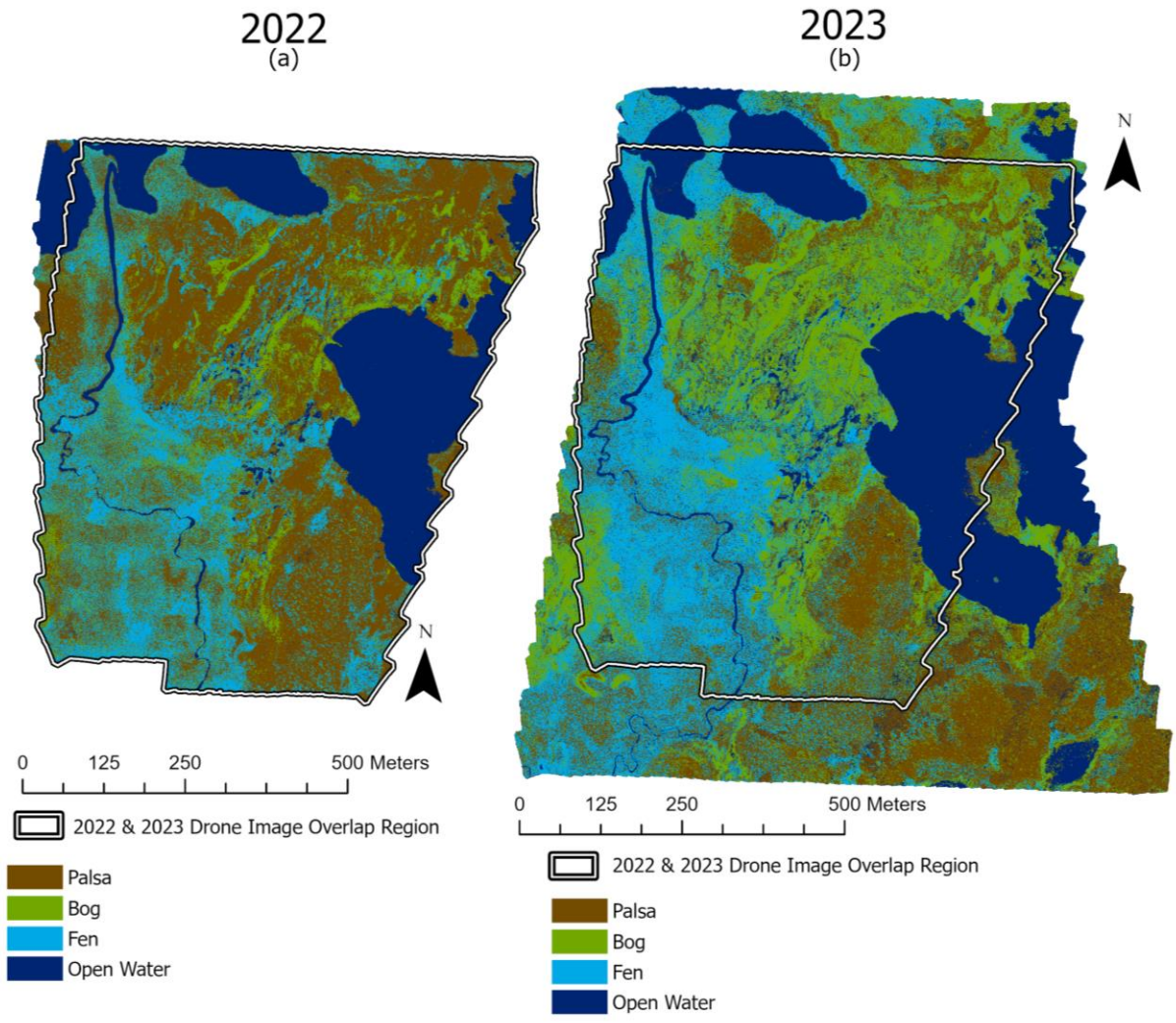

Figure 15a and 15b: Land Cover Classified Map of Stordalen Mire made in ArcGIS - Reclassed 2022 and 2023 images of Stordalen Mire created ArcGIS without the use of field spectrometers.

The classification analyses done in both GEE and ArcGIS use spectral unmixing as a point-based classifier as they use the components within a pixel to identify the land cover type present. One of the limitations to this method compared to an object-based classification is evident during the verification process, as it relies on a single pixel to determine whether a ground truth point is a hit or miss. An object-based classifier, on the other hand, uses image segmentation to create spectrally homogenous 'objects', the plots in this case (Jingxiao et al., 2014), and will use the most prominent signature in the object to determine hits and misses (Figure 16). In many cases of misclassification in this analysis, the surrounding area was correctly identified but the exact pixel was categorized as a different land cover. It is likely that aggregating the pixels before unmixing may account for some of this error.

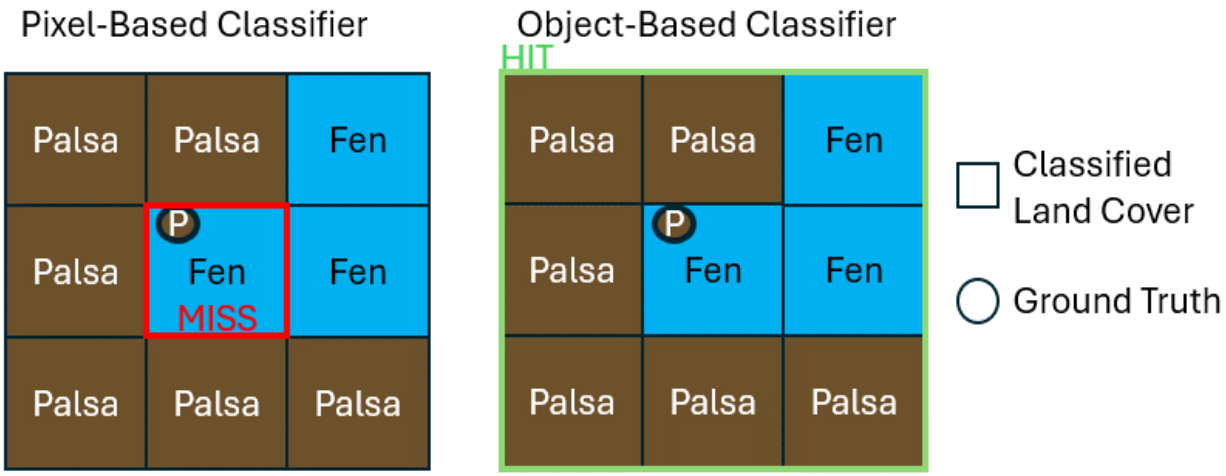

Figure 16 – Pixel-Based vs. Object-Based Classifiers: A comparison between the classifier verification between Pixel and Object Based Classifiers. Pixel-Based assess accuracy by using only the closest pixel to the ground truth site. Object-Based uses the overall classification of the entire plot (or designated 'object') to determine accuracy. The different assessment methods may result in different accuracy results.

Table 4: Accuracy of 2022 Reclassification Map made in ArcGIS -

Classification accuracies for 2022 land cover map created using a Random Trees Supervised Classification in ArcGIS Pro. The overall accuracy of this analysis was 77.1%. Similar to the 2022 GEE classifications, Open Water is overestimated, leading to a low consumer accuracy.

		Classification				
		Palsa	Bog	Fen	Open Water	Total
Reference	Palsa	19	2	3	1	25
	Bog	3	16	1		20
	Fen	3	2	15	1	21
	Open Water	0	0	0	4	4
	Total	25	20	19	6	70

	Producer Accuracy	Consumer Accuracy
Palsa	76.00%	76.00%
Bog	80.00%	80.00%
Fen	71.43%	78.95%
Open Water	100.00%	66.67%
	K-Hat	0.676
	Overall Accuracy	0.771

Table 5: Accuracy of 2023 Reclassification Map made in ArcGIS –

Classification accuracies for 2023 land cover map created using a Random Trees Supervised Classification in ArcGIS Pro. The overall accuracy is 78.6% with fens having the highest omission and commission error, meaning actual fens sites were missed and other sites were wrongfully classified as fens.

		Classification				
		Palsa	Bog	Fen	Open Water	Total
Reference	Palsa	19	2	2	1	24
	Bog	2	16	2		20
	Fen	2	2	14	1	19
	Open Water	0	0	1	6	7
	Total	23	20	19	8	70

	Producer Accuracy	Consumer Accuracy
Palsa	79.17%	82.61%
Bog	80.00%	80.00%
Fen	73.68%	73.68%
Open Water	85.71%	75.00%
	K-Hat	0.703
	Overall Accuracy	0.786

2.4 Cover Type Changes

2.4.1 Land Cover

Identifying land cover change and resulting biodiversity loss in GEE was done using the STELLA data due to the high accuracy of the classification maps. No change, meaning the land cover stayed the same, was by far the greatest area of the map, covering 12km (Figure 17, Table 6). Some of these class changes can be attributed to the higher misclassification of palsa and fen site as those are the areas with the most change. Additionally, the ‘thawed’ section in the lake is a result of a misclassification on the 2022 map (Figure 18a-d).

The purpose of creating these classification maps is not just to test the accuracy of these methods, but also to quantify the landscape changes in Stordalen Mire. Three methods of landscape change were analyzed based on the unique strengths of each classification tool: land cover changes based on thaw progression using the STELLA classifications, NDVI changes using drone imagery in ArcGIS, and change in individual species presence using the ColorSnap® tool. These methods for assessing landscape change can be used in conjunction with each other to fully understand an ecosystem’s response to climate change.

Land cover changes were monitored in terms of thaw progression and how the vegetation is changing as permafrost thaws and creates wetter conditions. The RedEdge spike of the EMR is a key distinguishing feature of the moisture content recorded at each site and identifying cover type. The main factors for determining cover type, which can be a subjective process, are canopy cover and species composition. The STELLA collected measurements accounted for both of these factors across the EMR. The most unchanged cover type across 2022-2023 was Open Water, which forms when thaw progression results in the creation of thaw ponds. On the other hand, palsa had the most new area, which is likely due to misclassification errors in the 2022 image, given it is the first stage of the thaw progression. Approximately three-quarters of the total bog area in 2022 was not classified as bog in 2023, meaning permafrost thaw is affecting bogs the most compared to the other cover types. However, a majority of the

bog changes (~60%) were reclassified to a palsa. This change may be accurately representing the landscape, but it is possible that error from the different wetness conditions of the 2 years studied or the differences in location from the drone. It is unclear the exact reason for the significant change in bog cover.

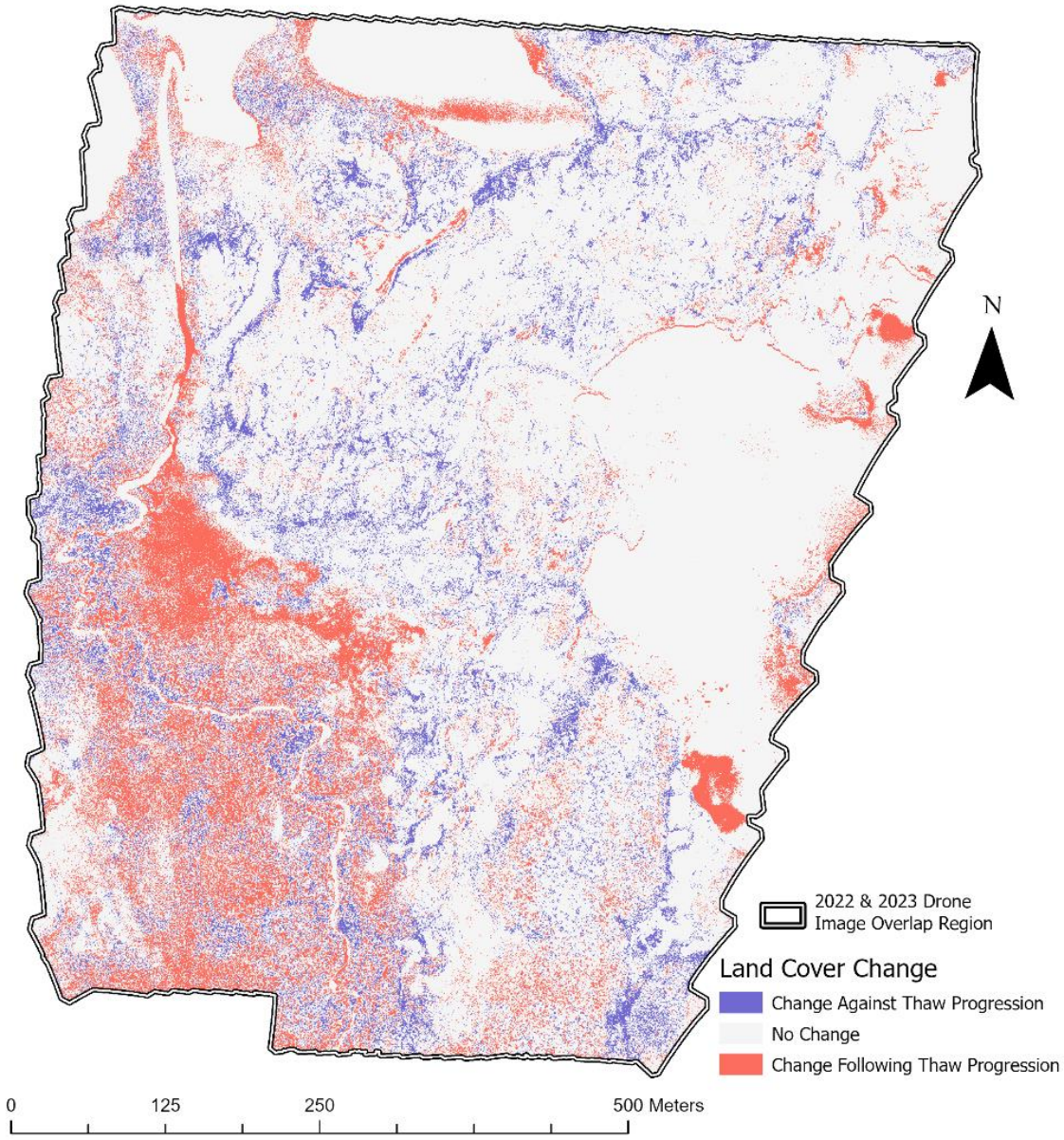

Figure 17: Land Cover Change from 2022 to 2023 - Map showing changes in land cover based on the GEE/STELLA reclassified images in terms of thaw progression. Changes that followed the thaw progression (e.g. palsa to bog), are identified as Thaw, were changes that went against the thaw progression (e.g. open water to fen), are shown as Reverse Thaw.

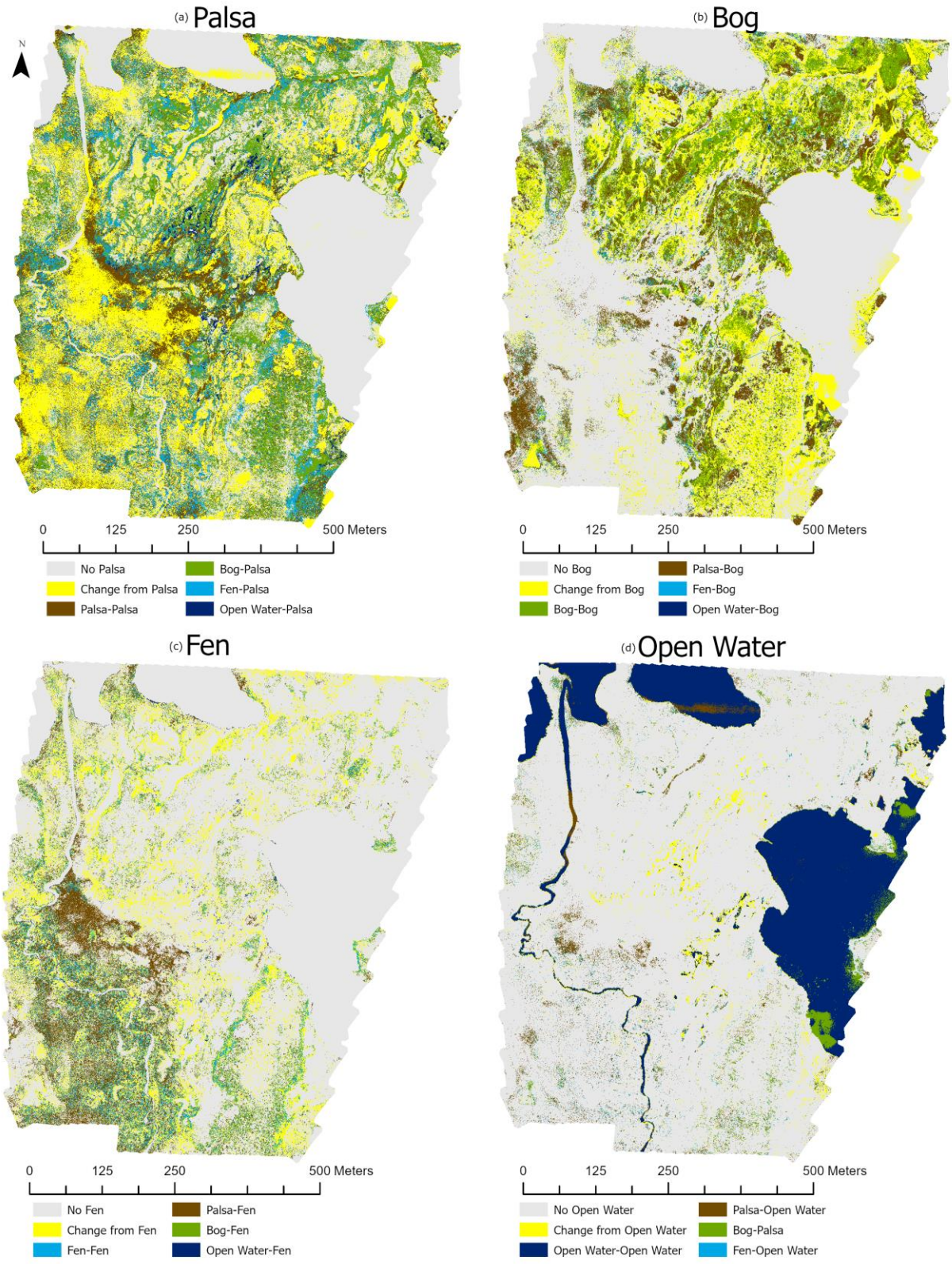
(a) Palsa
N
0
125
250
500 Meters
No Palsa
Change from Palsa
Palsa-Palsa
Bog-Palsa
Fen-Palsa
Open Water-Palsa
(b) Bog
0
125
250
500 Meters
No Bog
Change from Bog
Bog-Bog
Palsa-Bog
Fen-Bog
Open Water-Bog
(c) Fen
0
125
250
500 Meters
No Fen
Change from Fen
Fen-Fen
Palsa-Fen
Bog-Fen
Open Water-Fen
(d) Open Water
0
125
250
500 Meters
No Open Water
Change from Open Water
Open Water-Open Water
Palsa-Open Water
Bog-Palsa
Fen-Open Water

Figure 18a-d: Changes in Land Cover Type 2022-2023 Based on GEE/STELLA Reclassification - These maps show how the land cover has changed per cover type, and specifically which land cover type it was changed from.

Table 6: 2022-2023 Land Cover Changes: Changes in area for each land cover type between 2022 and 2023 in Stordalen Mire. The 'grayed-out' boxes along the diagonal show the area that remained the same for each land cover. Palsas covered the most new area and total area in 2023.

Land Cover Change (m^2)						
	From Palsa	From Bog	From Fen	From Open Water	Total New Area	Total Area 2023
New Palsa	3512.03	3969.36	2462.12	370.51	6801.99	10314.02
New Bog	3184.23	3003.85	721.68	126.27	4032.18	7036.03
New Fen	2400.22	728.13	1149.37	84.77	3213.13	4362.50
New Open Water	676.73	537.19	199.54	5024.95	1413.46	6438.41

2.4.2 NDVI

Change in photosynthetic material can vary in a region, especially during the growing season, so collecting imagery in the same phase is important for ensuring an accurate analysis. Figure 19 shows a range of least to most NDVI change, with significant change (>50% NDVI Loss) highlighted in red. This loss typically occurs in new fens, as land covers lose canopy cover and biodiversity. The areas with the least change in NDVI are land cover types that stayed the same, but remaining open water was the most consistent. This likely indicates that changes in NDVI are not due to land cover or species, but rather the impact of a wet 2022 and a dry 2023.

NDVI changes were analyzed in the ArcGIS Change Detection Model and are based on the Red and NIR bands of the 2022 and 2023 drone images. NDVI is measured on a -1 to 1 scale, and it is not uncommon to have variations in an area during a growing season. Additionally, only significant losses (>50%) in NDVI were selected to weed out any potential error from the growing season or interannual variation. The changes in NDVI are mostly attributed to changes in canopy cover, as land cover begins to transition to fens and thaw ponds, there is more open water and less vegetation, and as result, less photosynthetic material. The areas of significant NDVI loss correlate well with the area where palsa transitions to fen. This is another way to analyze the accuracy of the classification maps as this takeaway is expected. However, smaller scale thaw changes have been shown to lead to a temporary increase

in NDVI (Ogden et al., 2023) as the land cover transitions from palsa to sphagnum-dominated bog, which goes against other research showing that mosses are only capable of about one-third of primary production compared to vascular plants (Yuan et al., 2014). This analysis does not have a strong enough correlation to draw significant conclusions between NDVI changes and the palsa-bog-fen thaw gradient.

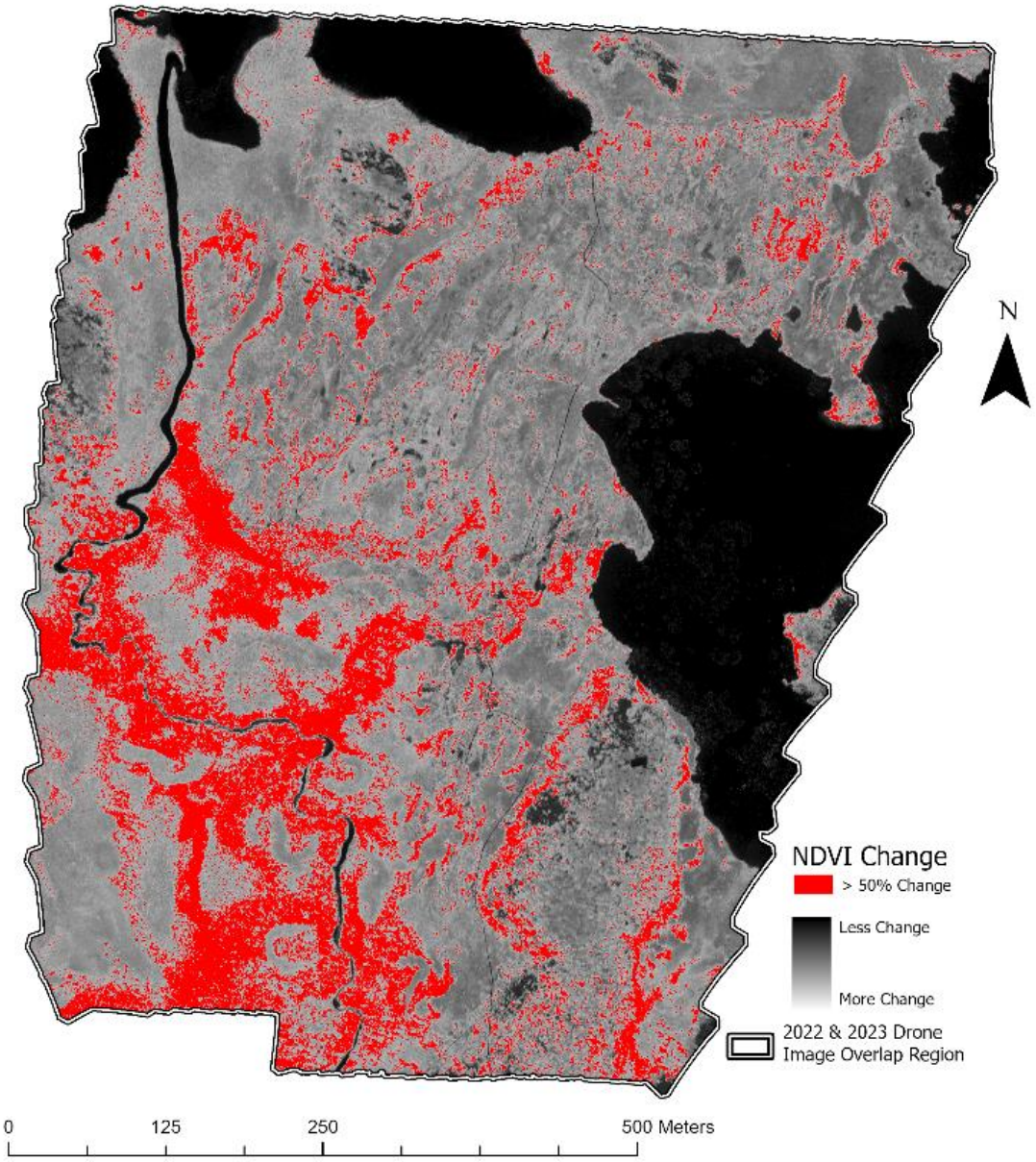

Figure 19: NDVI Change: At least 50% loss of photosynthetic material between 2022 and 2023 in Stordalen Mire is shown in red, over a black to-white gradient showing all NDVI change.

2.4.3 Species Change

Loss of individual species is and will continue to be a common case as permafrost thaw progresses and habitats become less suitable for several species. Lichen, for example, is a key moss species found in palsas and growing on rocks. Using the ColorSnap® to collect individual spectral signatures for Lichen as an endmember, Lichen composition maps were made for 2022 and 2023 and total loss can be compared (Figure 20, Table 7). In 2022, there was approximately 993m^2 area of lichen, but only 83m^2 in 2023 covering the same area. Vegetation plots monitoring species composition at this study site show similar trends (DeFelice, unpublished data, 2023). See Appendix D for the individual lichen composition maps for 2022 and 2023.

The ColorSnap® tool was effective in creating a species-level spectral library for identifying individual species change between 2022 and 2023. Lichen was chosen to illustrate this change as it can be a key indicator of ecosystem health (Ockinger et al., 2010) and a decline in its presence has been noted by field team members who have performed species composition regularly across these sites (DeFelice, unpublished data, 2023). Lichen decline shown in this research is comparable to other studies analyzing the relationship between climate change and lichen population (Stanton et al., 2023). As boreal ecosystems warm from climate change, the lichen population shifts and declines (Meyer et al., 2022).

Lichen was chosen specifically because of its noted decline during Mire-wide vegetation surveys across Stordalen (DeFelice, unpublished data, 2023). It is a unique case as it grows on rocks which should be unaffected by the landscape change occurring across the mire. This decline may be tied to grazing pressure by lemming, vole, or reindeer populations (Turunen et al., 2009) or lichen's high sensitivity to moisture compared to other species found in the area (Sandström et al., 2016). Either way, lichen appears to be a keystone species when determining the impacts of climate change in boreal ecosystems as its population is the first to decline during warmth (Meyer et al., 2022).

Table 7: Changes in Lichen Presence 2022-2023 – Total lichen coverage in 2022, 2023, and change between. Almost half of the lichen population from 2022 was lost in 2023.

Lichen Presence	Pixel Count	Total Area (m^2)
2022	156,879	910.9
2023	85,835	498.4
Both	14,220	82.6
Lichen Loss	71,044	412.5

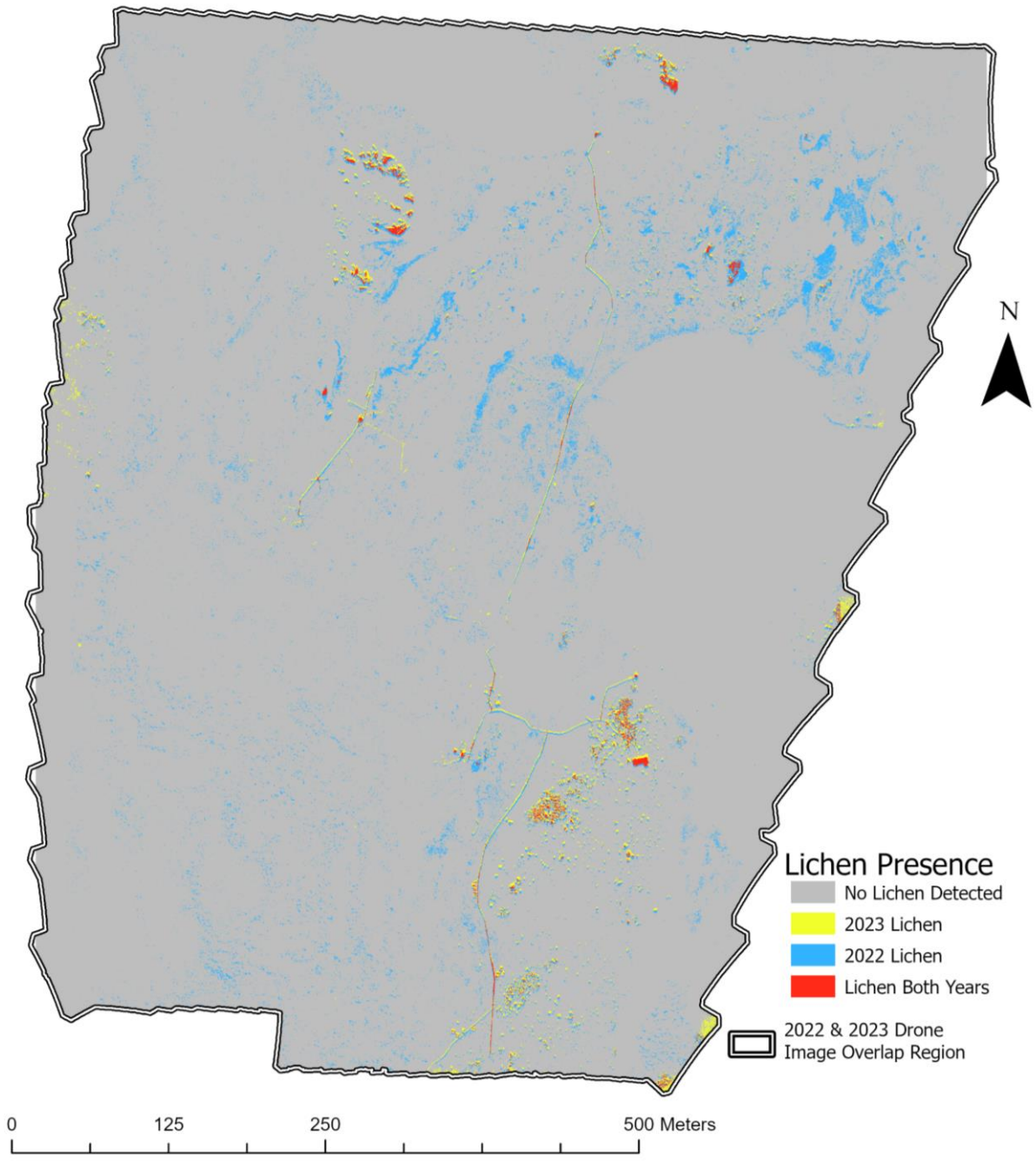

Figure 20: Lichen Change Detection 2022-2023: This map shows the distribution and changes in Lichen population from 2022-2023. There was almost a 60% loss of lichen between the two years.

CONCLUSIONS AND FUTURE WORK

Finding non-invasive, accurate ways to monitor landscape and biodiversity changes can require the use of multiple tools to ensure a comprehensive analysis is being performed and change is analyzed under every lens. This research utilized two low-cost spectrometers, the Sherwin-Williams® ColorSnap® and the NASA STELLA-Q, in conjunction with ArcGIS and GoogleEarth Engine software and drone aerial imagery to quantify species and land cover level changes from 2022 to 2023. This project presents and assesses the results of the landscape classifications through land cover change, NDVI loss, and change in individual presence, as well as the tradeoffs of these devices.

Image classification can be done at many levels based on the desired analysis and available resources. This research aimed to produce comprehensive analyses of sensitive ecosystems while comparing the functionality of inexpensive, field appropriate tools, including methods beyond tools' original purposes. The ColorSnap® is an effective tool for collecting spectral data for individual species and creating a spectral library, while the STELLA is better suited to collect at the land cover level. The combination of these tools allows for a comprehensive analysis of how an ecosystem is changing over time. These offer a cost-effective alternative to higher priced instruments, such as SVC and ASD spectrometers.

A large-scale, high species diverse study site such as Stordalen Mire proves difficult to accurately classify at the species-level using spectral unmixing, as only the species covering the most area in each pixel gets displayed and the spatial resolution of the drone imagery is greater than the leaf area for the species, which leads to many endmembers excluded from final classification maps. These factors combined to make it difficult to use species-level spectral measurements collected with the ColorSnap® for monitoring overall landscape changes over time, however monitoring the change in individual species presence was feasible.

As species-level classifications can be less reliable, it is common for researchers to create classes based on functional group or cover type and how they relate to biogeochemical processes, like permafrost collapse in this case, and many others in Arctic ecosystems. Other classifications in similar environments have been able to achieve similar classification accuracy without the use of field spectrometers, but in this case, the inclusion of the STELLA field spectrometer yielded higher accuracy (Palace et al., 2018).

Land cover level classification of Stordalen Mire was done in two ways: 1) Collecting endmember spectra using the NASA STELLA and reclassifying the drone imagery in GEE using spectral unmixing, and 2) Creating training sites in ArcGIS to reclassify the same drone image. Both methods were effective in producing maps with a high classification accuracy and low errors of omission and commission and were superior to classifications using the drone imagery alone.

The STELLA specifically is a very cost-effective field spectrometer and has produced higher classification accuracy and can be customized based on research interest and needs, which can lead to a more comprehensive data set with a small additional cost without requiring more work or collection. Customization of STELLA sensors can include air temperature, visible light in terms of brightness, air quality such as carbon dioxide and particulate matter, and other spectral sensors monitoring different bands of the EMR (STELLA Team, 2023). Since it was seen to increase classification accuracy in this analysis, it would be beneficial to equip several teams with STELLA devices to routinely collect ground-level spectral measurements to greatly increase the calibration and verification database.

This research shows that classification accuracy improves when ground truth measurements are collected in the same time frame as the aerial imagery, but it is possible that this is due to a relatively small sample size of each cover type. A repository of measurements collected across several years and at different stages of the growing season may allow for higher accuracy. Future work should include comparing the classification accuracy for all spectral measurements used as land cover

endmembers against just measurements collected alongside the aerial imagery. A more comprehensive analysis should also be done comparing these data to species level measurements collected with higher end spectrometers to identify any variation in reflectance or classification accuracy.

REFERENCES

Bäckstrand K, Crill PM, Jackowicz-Korczynski M, Mastepanov M, Christensen TR, Bastviken D. 2010. Annual carbon gas budget for a subarctic peatland, Northern Sweden. Biogeosciences 7:95-108. DOI:10.5194/bg-7-95-2010

Badulescu D, Simut R, Badulescu A, Badulescu AV. The Relative Effects of Economic Growth, Environmental Pollution and Non-Communicable Diseases on Health Expenditures in European Union Countries. Int J Environ Res Public Health. 2019 Dec 14;16(24):5115. doi: 10.3390/ijerph16245115. PMID: 31847367; PMCID: PMC6949912.

Bantilan-Smith, M., Bruland, G. L., MacKenzie, R. A., Henry, A. R., & Ryder, C. R. 2009. A comparison of the vegetation and soils of natural, restored, and created coastal lowland wetlands in hawai'i. *Wetlands*, *29*(3), 1023–1035. https://doi.org/10.1672/08-127.1

Bao, T., Jia, G., & Xu, X. (2022). Warming enhances dominance of vascular plants over cryptogams across northern wetlands. *Global Change Biology*, *28*(13), 4097-4109.

Berberoglu S, Lloyd CD, Atkinson PM, Curran PJ. (2000) The integration of spectral and textural information using neural networks for land cover mapping in the Mediterranean. Comput. Geosci 26:385–396

Bienau, M. J., Eckstein, R. L., Otte, A., & Durka, W. 2016. Clonality increases with snow depth in the Arctic dwarf shrub *empetrum hermaphroditum*. *American Journal of Botany*, *103*(12), 2105–2114. https://doi.org/10.3732/ajb.1600229

Bioucas-Dias, J.M.; Plaza, A.; Dobigeon, N.; Parente, M.; Du, Q.; Gader, P.; Chanussot, J. Hyperspectral Unmixing Overview: Geometrical, Statistical, and Sparse Regression-Based Approaches. *IEEE J. Sel. Top. Appl. Earth Obs. Remote Sens.*; 2012; *5*, pp. 354-379. [DOI: https://dx.doi.org/10.1109/JSTARS.2012.2194696]

Costa, J. J. F., Giasson, É., Da Silva, E. B., Tiecher, T., De Sena, A.,Francisco Sampaio, & e Silva, Ryshardson Geovane Pereira,De Oliveira. (2022). Soil

texture prediction through stratification of a regional soil spectral library. *Pedosphere, 32*(2), 294. https://doi.org/10.1016/S1002-0160(21)60074-7

DeFelice H, (2023). Species Composition in Stordalen Mire, Northern Sweden, 2023 [Dataset].

Environmental Science Research Institute (ESRI), (2023). ArcGIS Pro Version 3.2.0 [Computer Software]. Redlands, CA

Foody, G. M. (2002). Status of land cover classification accuracy assessment. *Remote Sensing of Environment*, *80*(1), 185–201. https://doi.org/10.1016/S0034-4257(01)00295-4

Gorelick, N., Hancher, M., Dixon, M., Ilyushchenko, S., Thau, D., & Moore, R. (2017). Google Earth Engine: Planetary-scale geospatial analysis for everyone. *Remote Sensing of Environment*.

T. A. Griffy, E. L. Hixson; Atmospheric acoustic noise as a function of altitude. *J. Acoust. Soc. Am.* 1 March 1989; 85 (3): 1089–1091. https://doi.org/10.1121/1.397492

Helander-Renvall, Elina. "Relationships between Sámi Reindeer Herders, Lands, and Reindeer." *Routledge Handbook of Human-Animal Studies; Routledge Handbook of Human-Animal Studies.* Edited by Garry Marvin, and Susan McHugh. Routledge/Taylor & Francis Group, 2014.

Huang, S., Tang, L., Hupy, J. P., Wang, Y., & Shao, G. (2020). A commentary review on the use of Normalized Difference Vegetation Index (NDVI) in the era of popular remote sensing. *Journal of Forestry Research*, *32*(1), 1–6. https://doi.org/10.1007/s11676-020-01155-1

Inga, B. (2007). Reindeer (Rangifer tarandus tarandus) feeding on lichens and mushrooms: traditional ecological knowledge among reindeer-herding Sami in northern Sweden. *Rangifer*, *27*(2), 93-106.

Johansson T, Malmer N, Crill PM, Friborg T, Åkerman JH, Mastepanov M, Christensen TR. 2006. Decadal vegetation changes in a northern peatland, greenhouse gas fluxes and net radiative forcing. Global Change Biology 12(12):2352–2369. DOI:10.1111/j.1365-2486.2006.01267.x

Jonasson C, Sonesson M, Christensen TR, Callaghan Tv. 2012. Environmental monitoring and research in the Abisko area-an overview. Ambio, 41(Suppl 3):178–186. DOI:10.1007/s13280-012-0301-6

J. Choi and K. Jo, "Attention based Object Classification for Drone Imagery," IECON 2021 – 47th Annual Conference of the IEEE Industrial Electronics Society, Toronto, ON, Canada, 2021, pp. 1-4, doi: 10.1109/IECON48115.2021.9589099.

Jingxiao Zhang, & Li Jia. (2014). A comparison of pixel-based and object-based land cover classification methods in an arid/semi-arid environment of Northwestern China. *2014 Third International Workshop on Earth Observation and Remote Sensing Applications (EORSA)*. https://doi.org/10.1109/eorsa.2014.6927922

Laporta, Gabriel Z., et al., "Biodiversity can Help Prevent Malaria Outbreaks in Tropical Forests: E2139." *PLoS Neglected Tropical Diseases*, vol. 7, no. 3, 2013, pp. e2139*. ProQuest*, https://ezproxy.rit.edu/login?url=https://www.proquest.com/scholarly-journals/biodiversity-can-help-prevent-malaria-outbreaks/docview/1327249127/se-2, doi:https://doi.org/10.1371/journal.pntd.0002139.

Malhotra A, Roulet NT. 2015. Environmental correlates of peatland carbon fluxes in a thawing landscape: do transitional thaw stages matter? Biogeosciences 12:3119–3130, DOI:10.5194/bg-12-3119-2015, 2015.

Malmer N, Johansson T, Olsrund M, Christensen TR. 2005. Vegetation, climate changes and net carbon sequestration in a North-Scandinavian subarctic mire over 30 years. Global Change Biology 11(11):1895-1909. DOI: 10.1111/j1365-2486.2005.01042.x

McCalley CK, Woodcroft BJ, Hodgkins SB, Wehr RA, Kim EH, Mondav R, Crill PM, Chanton JP, Rich VI, Tyson GW, Saleska, S. R. 2014. Methane dynamics regulated by microbial community response to permafrost thaw. Nature 514(7523):478–481. DOI:10.1038/nature13798

Meyer, A. R., Valentin, M., Liulevicius, L., McDonald, T. R., Nelsen, M. P., Pengra, J., … Stanton, D. 2023. Climate warming causes photobiont degradation and carbon starvation in a boreal climate sentinel lichen. *American Journal of Botany*, *110*(2), e16114. doi:10.1002/ajb2.16114

McHugh ML. Interrater reliability: the kappa statistic. Biochem Med (Zagreb). 2012;22(3):276-82. PMID: 23092060; PMCID: PMC3900052.

Ockinger, E., & Nilsson, S. G. 2010. Local population extinction and vitality of an epiphytic lichen in fragmented old-growth forest. *Ecology*, *91*(7), 2100–2109. doi:10.1890/09-1421.1

Ogden, E. L., Cumming, S. G., Smith, S. L., Turetsky, M. R., & Baltzer, J. L. 2023. Permafrost thaw induces short-term increase in vegetation productivity in northwestern Canada. *Global Change Biology*, *29*(18), 5352–5366. doi:10.1111/gcb.16812

Palace M, Herrick C, DelGreco J, Finnell D, Garnello AJ, McCalley C, McArthur K, Sullivan F, Varner RK. Determining Subarctic Peatland Vegetation Using an Unmanned Aerial System (UAS). *Remote Sensing*. 2018; 10(9):1498. https://doi.org/10.3390/rs10091498

Palace M, Herrick C, Sullivan F, Varner RK, Burke S, Cilento B, Pigott A, (2022). Unmanned Aerial Imagery over Stordalen Mire, Northern Sweden, 2022 [Data set].

Pontius, R. G., & Millones, M. (2011). Death to Kappa: birth of quantity disagreement and allocation disagreement for accuracy assessment. *International Journal of Remote Sensing*, *32*(15), 4407–4429. https://doi.org/10.1080/01431161.2011.552923

Reay, D. S., Smith, P., Christensen, T. R., James, R. H., & Clark, H. (2018). Methane and global environmental change. *Annual Review of Environment and Resources*, *43*, 165-192. https://doi.org/10.1146/annurev-environ-102017-030154

Roberts, D. A. (1991). *Separating spectral mixtures of vegetation and soils* (Order No. 9131704). Available from ProQuest Dissertations & Theses Global. (303965781).

Sandström, P., Cory, N., Svensson, J., Hedenås, H., Jougda, L., & Borchert, N. (2016). On the decline of ground lichen forests in the Swedish boreal landscape: Implications for reindeer husbandry and sustainable forest management. *Ambio*, *45*, 415-429.

SAS Institute, (2020-2021). JMP Pro Version 16.2.0 [Computer Software].

Sears, H. B., Palace, M. W., Sullivan, F., Herrick, C., Pardo, J., & Varner, R. K. (2023h).

Unmanned Aerial Imagery over Stordalen Mire, Northern Sweden, June 20, 2023 [Data set].

Shi, C. 2015. *Incorporating spatial information in spectral unmixing* (Order No. 3725991). Available from ProQuest Dissertations & Theses Global. (1733235198).

Stanton, D. E., Ormond, A., Koch, N. M., & Colesie, C. 2023. Lichen ecophysiology in a changing climate. *American Journal of Botany*, *110*(2), e16131. doi:10.1002/ajb2.16131

Szetela, J. 2023. *Into the Mire: A Floristic and Ecology Informed Field Guide of Stordalen Mire* (Order No. 30636712). Available from ProQuest Dissertations & Theses Global. (2854313196).

Tajibaeva, Liaila. *Integrated Economy of Humans and Biological Resources: A General Equilibrium Approach.* Federal Reserve Bank of St Louis, 2005.

Taylor, M., Mirel, P., Campbell, P., Barber, J., Walter, R., Williams. P., & Rayne, N. "STELLA Team." 2023. STELLA Spectrometers. https://landsat.gsfc.nasa.gov/stella/

Turunen, M., Soppela, P., Kinnunen, H., Sutinen, M.-L., & Martz, F. (2009). Does climate change influence the availability and quality of reindeer forage plants? *Polar Biology*, *32*(6), 813–832. https://doi.org/10.1007/s00300-009-0609-2

Varner RK, Crill PM, Frolking S, McCalley CK, Burke SA, Chanton JP, Holmes ME, Saleska S & Palace MW. 2022. Permafrost thaw driven changes in hydrology and vegetation cover increase trace gas emissions and climate forcing in Stordalen Mire from 1970 to 2014. Philosophical Transactions of the Royal Society A; Mathematical, Physical & Engineering Sciences 380(2215). DOI: 1-.1gl098/rsta.2021.0022

Xie, Y., Sha, Z., & Yu, M. 2008. Remote sensing imagery in vegetation mapping: A review. *Journal of Plant Ecology, 1*(1), 9-23. https://doi.org/10.1093/jpe/rtm005

Yuan, W., Liu, S., Dong, W., Liang, S., Zhao, S., Chen, J., … Vesala, T. 2014. Differentiating moss from higher plants is critical in studying the carbon cycle of the boreal biome. *Nature Communications*, *5*(1), 4270. doi:10.1038/ncomms5270

APPENDICIES

Appendix A: Comparison between Sherwin-Williams® ColorSnap®, NASA STELLA 1.0, and SVC HR-1024i-

	ColorSnap®	STELLA Q	HR-1024i
Cost	$60-80	~$275	~$30,000*
Diameter	4mm	~10cm	Customizable
Spectral Range	RGB*	450, 550, 570, 600, 610, 650, 680, 730, 760, 810, 860nm	350-2500nm
Size/Weight	1.08x2.17’ / 1 oz	~6.5x4.5’ /~ 1 lb.	8.75x11.5x3” / 8.5 lb.
Units	Digital Number	Radiance	Reflectance

Appendix B – List of Species Measured with ColorSnap® Tool and their Associated Land Covers

Endmember Name	Abbreviation	Distinction	Associated Land Cover
Andromeda polifolia	ANPO	Stem	Palsa
Andromeda polifolia	ANPOF	Inflorescence	Palsa
Aulocomium sp.	AUPO	*	Palsa
Betula nana	BENA	*	Palsa
Boardwalk	BW_W	Wet	*
Boardwalk	BW_W	Dry	*
Carex spp.	CASP	*	Fen
Carex spp.	CASPL	Litter	Fen
Dirt	DIRT	*	*
Empetrum hermaphroditum	EMHE	*	Palsa
Empetrum hermaphroditum	EMHEL	Litter	Palsa
Eriophorum angustifolium	ERAN	Tuft	Fen
Eriophorum russeolum	ERRU	Tuft	Fen
Eriophorum spp.	ERL	Litter	Fen
Eriophorum spp.	ERS	Stem	Fen
Eriophorum vaginatum	ERVA	Tuft	Fen
Lichen spp.	LICHG	Green	Palsa
Lichen spp.	LICHW	White	Palsa
Polytrichum spp	POSP	*	Palsa
Rock	ROCK	*	*
Rubus chamaemorus	RUCHF	Red Leaves	Palsa
Rubus chamaemorus	RUCH	*	Palsa
Salex spp.	SASPF	Catcin	Palsa
Salex spp.	SASP	*	Palsa
Sphagnum spp.	SPSPG	Green	Bog
Sphagnum spp.	SPSPA	Amber	Bog
Vaccinium microcarpum	VAMI	*	Palsa
Vaccinium uliginosum	VAUL	*	Palsa
Vaccinium uliginosum	VAULL	Litter	Palsa
Vaccinium vitis-idaea	VAVI	*	Palsa

Appendix C - Link to GEE Code for 2023 Land Cover Based Spectral Unmixing

https://code.earthengine.google.com/beeaf08431bd06dfa0f9ed38ed3bac4b

Appendix D - Lichen Presence in 2022 and 2023: